FEED AND BLEED IN PRESSURIZED WATER REACTORS ANALYZED UNDER UNCERTAINTY

by

VICTOR IANNELLO

SUBMITTED TO THE DEPARTMENT OF
NUCLEAR ENGINEERING
IN PARTIAL FULFILLMENT OF THE
REQUIREMENTS FOR THE DEGREES OF

MASTER OF SCIENCE

and

BACHELOR OF SCIENCE

in

NUCLEAR ENGINEERING

at the

MASSACHUSETTS INSTITUTE OF TECHNOLOGY

May 1984

© Victor Iannello 1984

The author hereby grants to M.I.T. and Associated Universities, Inc. permission to reproduce and to distribute copies of this thesis document in whole or in part.

Signature of Author _____
Department of Nuclear Engineering
May 11, 1984

Certified by _____
Neil E. Todreas
Professor of Nuclear Engineering

Accepted by _____
Allan Henry
Chairman, Departmental Graduate Committee

MASSACHUSETTS INSTITUTE OF TECHNOLOGY
AUG 07 1984
ARCHIVES
LIBRARIES

FEED AND BLEED IN PRESSURIZED WATER REACTORS ANALYZED UNDER UNCERTAINTY

by

VICTOR IANNELLO

Submitted to the Department of Nuclear Engineering on May 11, 1984 in partial fulfillment of the requirements for the Degrees of Master of Science and Bachelor of Science in Nuclear Engineering

ABSTRACT

A methodology to assess the primary feed and bleed process in pressurized water reactors (PWRs) subject to uncertainty in input parameters is presented. The study has three major sections. The first part develops the modeling of PWR subsystems, from which a fast-running code is created. The second part uses this code to perform a thermal hydraulic analysis of the feed and bleed procedure. The last part of the study examines how the transient calculation changes with variations in the input parameters.

Zion-1 was the PWR chosen on which to base this study. The scenario simulated was a loss-of-offsite power transient, followed by the failure of the operators to start the auxiliary feedwater pumps. The feed and bleed was assumed to be initiated 10 minutes after the loss-of-offsite power event.

Five parameters were then selected as significantly affecting whether the feed and bleed would be successful. A response surface was generated as a function of these input parameters. The five parameters were then treated as continuous random variables, and probability density functions were chosen to describe their uncertainties. A Monte Carlo simulation using the response surface and distributions was then performed to determine the probability of successfully cooling the core using the feed and bleed procedure.

Thesis Supervisor: Dr. Neil E. Todreas

Title: Head, Department of Nuclear Engineering

DEDICATION

To my parents, Anthony and Beatrice, whose love and support made this work possible.

ACKNOWLEDGEMENTS

The research for this thesis was performed while I was associated with the Risk Assessment Division in the Department of Nuclear Energy at Brookhaven National Laboratory. I would like to thank the entire Risk Evaluation Group for their continued support and valuable comments. In particular, I gratefully acknowledge the assistance given to me by Dr. Robert W. Youngblood, who spent many hours of his time discussing his thoughts about my work with me, and the recommendations of Dr. Ioannis A. Papazoglou, who served as my thesis supervisor while I was at BNL. I would aslo like to thank Ms. Denise Miesell for her assistance in the production of the manuscript.

I am also grateful to Professor Neil E. Todreas, my thesis advisor, who carefully reviewed this study and provided me with many insightful comments.

TABLE OF CONTENTS

FIGURES

TABLES

Section 1

INTRODUCTION

After a reactor scram, there is still some energy release caused by the decay of the fission products. This so-called "decay power" diminishes to only a few percent of the total reactor power within a short time after the fission process has been stopped; however, this decay power is long-lived. The decay power following a sustained constant power operation of a reactor falls off only as time raised to the negative one-fifth power. As a result, for a reactor operating in the several thousand megawatt range, the decay power, when integrated over time, represents an appreciable amount of energy. Systems are thus designed to remove this decay power from the core.

In the event of a scram in a pressurized water reactor (PWR), the steam generators are relied on to remove the decay heat from the reactor coolant system. Heat is transferred from the primary to the secondary side of the steam generators. The seconday side, being at lower pressure than the primary side, will boil. The auxiliary feedwater system is designed to replace this liquid boiled off so that the water level on the secondary side remains between some pre-determined setpoints.

An accident in which both main and auxiliary feedwater systems are not available is called a loss-of-feedwater (LOFW) accident. In this event, secondary water inventory is boiled off and not replaced and thus the water level decreases. As the level decreases, the primary to secondary heat transfer is degraded, and eventually the steam generators will transfer little or no heat from the primary. There now exists a situation in which energy is added to the primary system by the core and is not removed.

Feed and bleed might be initiated in this accident as a final effort to prevent the core from melting. In this mode of cooling, liquid is injected via the emergency core cooling system (ECCS) into the core. Fluid is removed from the primary coolant system through the pressurizer power-

operated relief valves (PORVs), as shown in Fig. 1-1. As the fluid flows through the core, it is heated. In this manner, the fluid flow will remove energy from the primary coolant system.

Currently, there is a great deal of interest in determining if the feed and bleed process will successfully cool the core. The answer strongly depends on plant specific parameters such as the ECCS capacity, PORV relief capacities, and core power levels. A general statement about the effectiveness of the feed and bleed process cannot be made.

There have been several studies on specific plants. Los Alamos has studied LOFW transients for the Zion-1 PWR (Ref.4). The results show that feed and bleed will successfully cool the core if initiated within 10 minutes with full ECC capacity. Babcock and Wilcox has performed a feed and bleed analysis on a system representative of their 177-FA lowered-loop plants (Ref.15). Their results show that the core can be successfully cooled by using one of the two high pressure injection pumps if the ECC injection is initiated within 20 minutes.

Things are more complicated for most Combustion Engineering plants. These plants lack sufficient injection capacity at the setpoint pressure of PORVs to cool the core. Instead, the plants must first depressurize to a pressure at which the ECC flow capacity can sufficiently cool the core. This method of core cooling is referred to as "bleed and feed" since the primary system inventory must be sufficiently bled before adequate ECC flow can be injected. Since in this mode the PORVs are latched open to depressurize the system, excessive coolant mass may be removed and the core may uncover before the pressure decreases sufficiently for the ECC injection to add as much coolant to the primary as is flowing out the PORVs.

An experiment at the Loss-of-Fluid Test (LOFT) facility at Idaho National Engineering Laboratory (experiment LP-FW-1) was conducted to simulate a LOFW transient and recovery using bleed and feed (Ref.11). The conclusions indicate that primary feed and bleed was highly effective in recovering from the transient when the PORVs were latched open. ECC flow exceeded PORV flow before the core was uncovered.

The purpose of this study is to examine the feed and bleed process in PWRs in a probabilistic manner. Although the best estimate calculations performed so far have indicated that feed and bleed can successfully cool the core, this study examines how this answer might change when the input parameters vary from the values chosen in the best-estimate predictions. These parameters vary either because our knowledge of the quantities is incomplete or because the parameter is inherently uncertain. For instance, the flow that an individual pump delivers at a given pressure might vary from that value determined from its head-flow curve. The variation is due to our incomplete knowledge of the environment in which the pump operates, its maintenance schedule, age, etc. On the other hand, a parameter that describes operator action is inherently uncertain. These input parameters were considered to be random variables and assigned range of values and associated probabilities. The uncertainties associated with these input parameters were then propagated to determine how they change our predictions of the feed and bleed scenario from the best-estimate predictions.

Zion-1 was chosen as the plant on which to base the study. This is a four loop Westinghouse plant owned and operated by Commonwealth Edison. The plant has two safety-grade centrifugal charging pumps (CCPs) as part of its ECCS. As a result, depressurization would not be necessary for a manual initiation of safety injection.

This study is divided into three main parts. The first consists of the modeling of the relevant parts of a PWR system necessary for the feed and bleed thermal hydraulic analysis. The modeling was used to develop a fast running transient analysis code called FABREC (Feed and Bleed RESponse Code).

The second part of the study examines the thermal hydraulic aspects of the feed and bleed process. FABREC is used to predict the system response to a loss-of-feedwater transient followed by failure of ECC system in one scenario, and primary feed and bleed in another. These results are then compared with those calculated in Ref.4, which used TRAC (Transient Reactor Analysis Code) for its simulation.

The last part of the study examines how the transient calculation changes with variations in the input parameters. An output variable was first chosen with which to judge the success of the feed and bleed process. A response surface as a function of selected input parameters was then generated. After pdfs for the input parameters were chosen, a Monte Carlo simulation was performed using the generated response surface. Finally, the distribution from the Monte Carlo simulation was fitted to a two-parameter pdf using moment-matching methods.

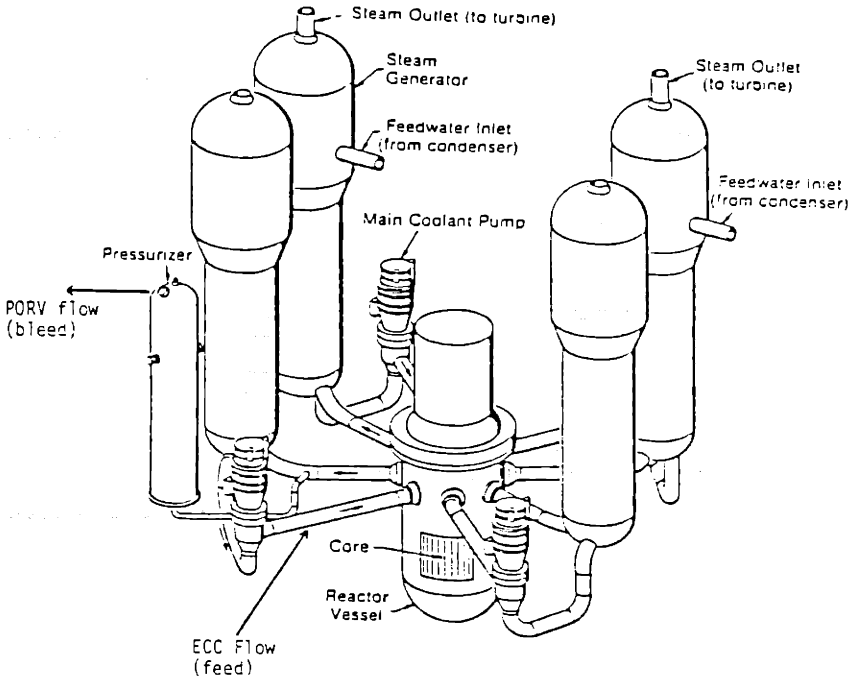

Figure 1-1 Feed and bleed in a PWR. (Adapted from a Westinghouse drawing)

Section 2

MODELING OF PWR SUBSYSTEMS

2.1 Introduction

In order to simulate feed and bleed in PWRs, a computer code was developed. The main criteria for the code was that it be fast running (several times faster than real time) and easy to use. The result of this effort is the Feed and Bleed Response Code (FABREC). It is written in Fortran IV and can be compiled and run on either the CDC-6600 or CDC-7600.

Figure 2-1 shows the noding scheme used in FABREC. Six nodes are used to model a PWR. The core, upper plenum, lower plenum, and pressurizer each are modeled as one node. One node is also used to model the hot and cold legs of the reactor coolant system and the primary side of the steam generators. The remaining node models the secondary side of the steam generators. Thus, the symmetry of a multi-loop PWR is utilized to reduce the number of nodes necessary to model the out of core components.

Another large reduction in the running time of FABREC was accomplished by the elimination of the momentum equation. In its place, an empirical expression for the steady-state total loop pressure drop is used. The reactor coolant system is assumed to be at uniform pressure equal to that of the pressurizer. As a result, the integration scheme employed is totally explicit. The time step size is thus monitored to prevent numerical instabilities.

FABREC assumes instantaneous phase separation in the pressurizer (infinite bubble rise velocity). Under accident conditions, it is possible that the water in the reactor vessel will also start to void. For these conditions, the code assumes homogeneous flow in the core and phase separation in the upper plenum. The vapor and liquid are assumed to be in thermal equilibrium in any node where two-phase conditions are present.

Although the code is very simple, it can model the relevant sequences in a feed and bleed scenario. The code can predict such phenomena as steam generator dryout time, natural circulation flow rates, and decay power levels. Because it is fast running, it is ideal for sensitivity studies.

2.2 Generalized Equations for Nodes with Pressure Boundary Conditions

There are basically two types of nodes in FABREC. Type I nodes have their inlet flow and average pressure specified. The node outlet flow is calculated. A Type II node has both its inlet and outlet flows specified. In this case, the average node pressure is calculated. All the nodes in FABREC are Type I except for the pressurizer and the steam generator secondaries before the relief valves open. The Type II nodes determine the primary and secondary pressures.

Let us first consider the nodes where the pressure is specified (Type I). Figure 2-2 represents a control volume that experiences both energy and mass transfer. Our goal is to uncouple the mass and energy equations so that the node outlet flow and enthalpy can be calculated. Let's first write down the mass equation for this control volume:

$$\frac{dm}{dt} = \dot{m}_{in} - \dot{m}_{out}. \qquad (2.02\text{-}1)$$

We can also write down the energy equation for this control volume as

$$\frac{d(mu)}{dt} = \dot{m}_{in}h_{in} - \dot{m}_{out}h_{out} + \dot{Q}. \qquad (2.02\text{-}2)$$

Work is not included in (2.02-2) because the control volume is considered rigid and thus experiences zero boundary work. Shaft work is neglected because there are no shaft work devices present.

Our first assumption is that the rate of change of the node-averaged internal energy, u, can be approximated by that of the node-averaged enthalpy, h*. This is equivalent to saying that we will neglect the rate of change of flow work in our energy equation. Equation (2.02-2) now becomes

$$\frac{d(mh)}{dt} = \dot{m}_{in}h_{in} - \dot{m}_{out}h_{out} + \dot{Q} \qquad (2.02\text{-}3)$$

*The term "enthalpy" as used in this study is synonymous with "specific enthalpy" and has the same units as internal energy, i.e., energy per unit mass.

Our second assumption is that the rate of change of the outlet enthalpy equals that of the node-averaged enthalpy. This is an assumption common to many codes. Equation (2.02-3) can now be written as

$$\frac{d(mh_{out})}{dt} = \dot{m}_{in}h_{in} - \dot{m}_{out}h_{out} + \dot{Q}. \qquad (2.02\text{-}4)$$

We can also expand the left-hand side of (2.03-4) and substitute in (2.02-1) to obtain

$$h_{out}[\dot{m}_{in}-\dot{m}_{out}] + m\frac{dh_{out}}{dt} = \dot{m}_{in}h_{in} - \dot{m}_{out}h_{out} + \dot{Q}. \qquad (2.02\text{-}5)$$

Rearranging (2.02-5), and making use of our second assumption about $\frac{dh_{out}}{dt}$, we can say

$$\frac{dh}{dt} = \frac{\dot{m}_{in}(h_{in}-h_{out}) + \dot{Q}}{m}. \qquad (2.02\text{-}6)$$

Remember, we set out to derive an expression for both the outlet enthalpy and flow for a Type I node. We still do not have an expression for the outlet flow rate.

One method to find the outlet flow rate is to consider the volume constraint. We know that

$$m = \rho V. \qquad (2.02\text{-}7)$$

Differentiating (2.02-7) produces

$$\frac{dm}{dt} = \frac{\rho dV}{dt} + \frac{V d\rho}{dt}. \qquad (2.02\text{-}8)$$

As stated previously, our control volume is rigid so that we can eliminate the first term of (2.02-8) and write

$$\frac{dm}{dt} = \frac{V d\rho}{dt}. \qquad (2.02\text{-}9)$$

We know that the state of a pure substance is completely determined by two thermodynamic properties. Thus, the density is a function of enthalpy and pressure. Expanding the rate of change of the density using a first-order Taylor series approximation results in

$$\frac{d\rho}{dt} \simeq \left(\frac{\partial \rho}{\partial h}\right)_p \frac{dh}{dt} + \left(\frac{\partial \rho}{\partial p}\right)_h \frac{dp}{dt} \quad . \tag{2.02-10}$$

Our third assumption is that the fluid is incompressible, i.e., $\left(\frac{\partial \rho}{\partial p}\right)_h \simeq 0$.

Combining (2.02-9) and (2.02-10), and using our assumptions about fluid incompressibility and rate of change of outlet enthalpies, produces

$$\frac{dm}{dt} = V\left(\frac{\partial \rho}{\partial h}\right)_p \frac{dh}{dt} \quad , \tag{2.02-11}$$

which can be set equal to (2.02-1) and solved for $\dot{m}_{out}$ to yield

$$\dot{m}_{out} = \dot{m}_{in} - V\left(\frac{\partial \rho}{\partial h}\right)_p \frac{dh}{dt} \quad . \tag{2.02-12}$$

One more relation must be discussed before the number of unknowns in the node balances the number of equations. An expression relating the node average enthalpy to the enthalpy leaving the node is desired. If the nodes are small, one can assume the node is well mixed such that the enthalpy leaving the node is equal to the average node enthalpy. In FABREC, however, the nodes are quite large. An enthalpy distribution is thus assumed. The distribution assumed depends both on the type of node and thermodynamic conditions present. For instance, the enthalpy leaving the upper plenum equals the node-averaged enthalpy for single phase conditions, but the same statement cannot be made once the plenum saturates and experiences phase separation.

The equations listed below are equations solved in Type I nodes to calculate the thermodynamic conditions present as well as outlet flows and

enthalpy. The pressure, p*, is calculated by a Type II node and input to the Type I node.

$$\frac{dh}{dt} = \frac{\dot{m}_{in}(h_{in}-h_{out}) + \dot{Q}}{m} \qquad \text{(modified energy equation)}, \qquad (2.02\text{-}6)$$

$$\dot{m}_{out} = \dot{m}_{in} - \left(\frac{\partial\rho}{\partial h}\right)_p \frac{dh}{dt} \qquad \text{(modified mass equation)}, \qquad (2.02\text{-}12)$$

$$h_{out} = f(h_{in},h) \qquad \text{(enthalpy distribution)}, \qquad (2.02\text{-}13)$$

$$\rho = \rho(h,p^*) \qquad \text{(equation of state)}, \qquad (2.02\text{-}14)$$

$$m = \rho V. \qquad \text{(volume constraint)}. \qquad (2.02\text{-}7)$$

The assumptions needed to derive these equations were:

1) Neglect flow work,

2) Rate of change of outlet enthalpy equals rate of change of node-averaged enthalpy, and

3) Fluid is incompressible $\left(\left(\frac{\partial\rho}{\partial p}\right)_h \simeq 0\right)$.

2.3 Lower Plenum

The lower plenum is represented as a Type I node in FABREC. Thus, the inlet flow and enthalpy and pressure are specified. All the nodes representing the reactor coolant system are at the pressure of the pressurizer, which is represented by a Type II node. The Type II node thus determines the pressure for all the Type I nodes.

Table 2.1 explains what the variables used for the lower plenum equations represent. Examining Figure 2-1, we see that flow enters the lower plenum from both the cold leg and from ECC injection. The water that leaves the lower plenum enters the core region. We can assume the lower plenum is adiabatic so that it experiences no heat transfer. We also assume that as water enters the plenum it is perfectly and instantaneously mixed with the water already present. Referencing (2.02-6, 7, 12, 13, and 14) the equations for the lower plenum can be written as

$$\frac{dh_\ell}{dt} = \frac{\dot{m}_{i\ell}(h_{i\ell}-h_{\ell c}) + \dot{m}_{s\ell}(h_{s\ell}-h_{\ell c})}{m_\ell} , \qquad (2.03\text{-}1)$$

$$\dot{m}_{\ell c} = \dot{m}_{i\ell} + \dot{m}_{s\ell} - V_\ell \left(\frac{\partial \rho}{\partial h}\right)_p \frac{dh_\ell}{dt} , \qquad (2.03\text{-}2)$$

$$h_{\ell c} = h_\ell , \qquad (2.03\text{-}3)$$

$$\rho_\ell = \rho(h_\ell, p^*) , \qquad (2.04\text{-}4)$$

$$m_\ell = \rho_\ell V_\ell . \qquad (2.05\text{-}5)$$

2.4 Core

The core is represented by a single Type I node in FABREC. Thus, the inlet flow and enthalpy are known. The pressure of the core is assumed equal to that of the pressurizer. Table 2.2 defines the variables used in the core equations.

Unlike the lower plenum, we assume the enthalpy leaving the core does not equal the node-average enthalpy. At steady-state conditions and symmetric power distribution about the core mid-plane, the average enthalpy of the water in the core is the simple arithmetic average of the inlet and outlet enthalpies. This is the distribution we will assume for our core. We can thus write

$$h_c = \frac{h_{\ell c} + h_{cu}}{2} \quad , \tag{2.04-1}$$

or,

$$h_{cu} = (2)(h_c) - h_{\ell c} \quad . \tag{2.04-2}$$

In the case of two-phase conditions in the core, this assumption implies a homogeneous, equilibrium flow. No phase separation is assumed to occur.

We can now write down the equations for the core node as

$$\frac{dh_c}{dt} = \frac{\dot{m}_{\ell c}(h_{\ell c} - h_{cu}) + \dot{Q}_{core}}{m_c} \quad , \tag{2.04-3}$$

$$\dot{m}_{cu} = \dot{m}_{\ell c} - V_c \left(\frac{\partial \rho}{\partial h}\right)_p \frac{dh_c}{dt} \quad , \tag{2.04-4}$$

$$h_{cu} = (2)(h_c) - h_{\ell c} \quad , \tag{2.04-2}$$

$$\rho_c = \rho(h_c, p^*) \quad , \tag{2.04-5}$$

$$m_c = \rho_c V_c \quad . \tag{2.05-6}$$

2.5 Upper Plenum

The upper plenum node is connected to the core on one end and both the pressurizer and steam generator on the other. Since a Type I node will only calculate one outlet flow rate, the question becomes how to determine the flow split between the steam generator and the pressurizer. For now, let's assume we know the flow entering the steam generator so that the surge entering the pressurizer can be calculated if the total outlet flow is known. Later, the procedure for calculating the flow entering the steam generators will be shown.

Figure 2-3 shows a schematic representation of the upper plenum. Notice the hot leg nozzle is well below the head of the vessel. This will become important when two-phase conditions are present in the primary system. Table 2.3 lists the variables used for the upper plenum equations.

It is assumed that for single phase conditions, the upper plenum is perfectly and instantaneously mixed such that

$$h_{us} = h_u \quad . \tag{2.05-1}$$

For two-phase conditions, things get a bit more complicated. The assumption is that there is complete and instantaneous phase separation in the upper plenum. For a mixture level that is below the hot leg nozzle, saturated steam is assumed to exit the plenum. For a mixture level completely above the hot leg nozzle, saturated liquid exits the plenum. For a mixture level somewhere between the two, a two-phase flow is assumed to exit. The two-phase flow exiting the plenum is considered to be homogeneous and in thermal equilibrium such that the void fraction is the cross-sectional area of the steam divided by the cross-sectional area of the nozzle (Figure 2-4). We can write this as

$$\alpha = \frac{A_g}{A_n} \quad . \tag{2.05-2}$$

Once we know the void fraction, we can calculate the cross-sectional averaged enthalpy. Let's first write down expressions for the liquid and steam mass flow rates through the nozzle.

$$\dot{m}_f = \rho_f w A_f \tag{2.05-3}$$

$$= \rho_f w(1-\alpha)A_n \tag{2.05-4}$$

$$\dot{m}_g = \rho_g w A_g \tag{2.05-5}$$

$$= \rho_g w \alpha A_n \tag{2.05-6}$$

The homogeneous equilibrium flow enthalpy leaving the plenum is thus

$$h_{us} = \frac{\dot{m}_f h_f + \dot{m}_g h_g}{\dot{m}_f + \dot{m}_g} , \tag{2.05-7}$$

$$= \frac{\rho_f w(1-\alpha)A_n h_f + \rho_g w \alpha A_n h_g}{\rho_f w(1-\alpha)A_n + \rho_g w \alpha A_n} , \tag{2.05-8}$$

$$h_{us} = \frac{\rho_f(1-\alpha)h_f + \rho_g \alpha h_g}{\rho_f(1-\alpha) + \rho_g \alpha} . \tag{2.05-9}$$

Thus, for saturated conditions in the plenum, the outlet enthalpy is calculated by first finding the void fraction of flow exiting and substituting into (2.05-9). For single phase conditions, the enthalpy leaving equals the node-averaged enthalpy. The upper plenum equations are, therefore,

$$\frac{dh_u}{dt} = \frac{\dot{m}_{cu}(h_{cu}-h_{us})}{m_u} , \tag{2.05-10}$$

$$\dot{m}_{up} = \dot{m}_{cu} - \dot{m}_{us} - V_u\left(\frac{\partial \rho}{\partial h}\right)_p \frac{dh_u}{dt} , \tag{2.05-11}$$

$$h_{us} = \begin{cases} h_u & \text{Single phase upper plenum} \\ \dfrac{\rho_f(1-\alpha)h_f + \rho_g\alpha h_g}{\rho_f(1-\alpha) + \rho_g\alpha} & \text{Two-phase upper plenum} \end{cases} \quad (2.05\text{-}12)$$

$$\alpha = \frac{A_g}{A_n} , \quad (2.05\text{-}2)$$

$$\rho_u = \rho(h_u, p^*) , \quad (2.05\text{-}13)$$

$$m_u = \rho_u V_u . \quad (2.05\text{-}14)$$

2.6 Steam Generator Primary Side

In FABREC, a single node represents the hot and cold legs of the reactor coolant system, and the primary side of the steam generators. For identification purposes, we will refer to this node as the steam generator primary with the understanding that it also includes the hot and cold leg piping. Although most of the important phenomena do actually occur in the steam generators, the piping is of considerable volume so that the large mass of water contained in the pipes becomes important under transient conditions.

The steam generator primaries are represented by a Type I node. Table 2.4 lists the representation of variables used in the steam generator primary equations, which are

$$\frac{dh_s}{dt} = \frac{\dot{m}_s(h_{us}-h_s)-\dot{Q}_{sg}}{m_{st1}} \quad , \tag{2.06-1}$$

$$\frac{dm_{st1}}{dt} = V_s\left(\frac{\partial\rho}{\partial h}\right)_p \frac{dh_s}{dt} \quad , \tag{2.06-2}$$

$$\dot{m}_{s\ell} = \dot{m}_s - \frac{dm_{st1}}{dt} \quad . \tag{2.06-3}$$

2.7 Primary-to-Secondary Heat Transfer

The steam generator heat transfer model used is FABREC is a modification of that used in the MARCH code (Ref.22). The model assumes that the overall heat transfer can be approximated by multiplying its full-power, steady-state value by two correction factors. The heat transfer equation is similar to that used to size standard heat exchangers. It can be written as

$$\dot{Q}_{sg} = UA\Delta T_{\ell m} \ , \qquad (2.07\text{-}1)$$

where

$$\Delta T_{\ell m} = \frac{(T_u - T_2) - (T_s - T_2)}{\ln \dfrac{T_s - T_2}{T_s - T_2}} \ , \qquad (2.07\text{-}2)$$

where T_u, T_s, and T_2 are temperatures of the hot leg, cold leg, and secondary side, respectively. If one knows the full-power log mean temperature difference, $\Delta T_{\ell m_o}$, and the full-power heat transfer rate, $\dot{Q}_{sg_o}$ (which equals the core power at full-power steady-state), the full-power heat transfer coefficient can be solved by the equation

$$(UA)_o = \frac{\dot{Q}_{sg_o}}{\Delta T_{\ell m_o}} \ . \qquad (2.07\text{-}3)$$

The first correction factor in determining (UA) from $(UA)_o$ accounts for voiding of the secondary side water inventory. The simple model says that as the water on the secondary side boils away, more of the steam generator tube area is uncovered. Remember, phase separation is assumed to occur on the secondary side. If we assume that the heat transfer to the steam is negligible, then the effective heat transfer area is proportional to the mass of liquid remaining on the secondary side, m_{st}.

The second correction factor accounts for the change in the heat transfer coefficient with temperature changes. For pool boiling, researchers have proposed that

$$h \sim \Delta T^n, \qquad (2.07\text{-}2)$$

where n ranges from 0.25 to 2, depending on the correlation used. In FABREC, it is assumed that his exponent equals 0.333, which is the same value used in the MARCH code. Rewriting (2.07-1) substituting for (UA) yields

$$\dot{Q}_{sg} = (UA)_o \left(\frac{m_{st}}{m_{sto}}\right) \left(\frac{\Delta T_{\ell m}}{\Delta T_{\ell m_o}}\right)^{1/3} \Delta T_{\ell m} \quad . \qquad (2.07\text{-}3)$$

2.8 Loop Flow Rate

Because all the loops of a multi-loop pressurized water reactor are represented as a single loop in FABREC, only sequences in which all the loops experience identical transients may be simulated. If one of four reactor coolant pumps trips in a four loop design, for instance, there would exist an asymmetric flow distribution. In fact, the loop that had the pump trip would actually experience a flow reversal. The driving force for the flow reversal would be the head developed by the other three operating pumps. FABREC could not accurately predict such a transient.

In order to calculate the loop flow rate, FABREC divides the flow into three separate regimes. When the pumps are operating, the loop is in the forced convection regime. With the advent of a pump trip, the loop begins a coastdown. After coastdown, natural circulation continues to drive the flow.

FABREC assumes that as long as the pumps are running, the flow is equal to that for full-power operation. This is not a bad assumption if the primary water properties do not change significantly for different power levels. For subcooled water, the assumption is valid.

After the pumps trip, the flow starts a coastdown. The rate of coastdown is governed by the geometry of the loop and the inertia of the pump. FABREC assumes an exponential coastdown which has a time constant that is input. The time constant for a particular reactor can be obtained from the coastdown curves listed in its FSAR.

The natural circulation model is very simplified. The driving force for the natural convection is the height difference between the thermal centers of the core and steam generators, which generates a gravity head. Flow resistance is the opposing force.

As stated previously, FABREC never solves the full momentum equation. Instead, a quasi-steady solution is sought. Empirical expressions are used to calculate the flow pressure drop and gravity pressure rise. For quasi-steady conditions, the two must balance. Thus, if we know the relationship between friction pressure drop and loop flow rate, we can solve the latter for a given gravity head. This is the basic procedure FABREC uses to calculate the loop flow rate.

Let us first derive an expression for the gravity head. If the thermal center height difference between the core and steam generators is ΔZ, then the pressure rise in the loop due to the density difference of the water leaving the core and water leaving the steam generators is

$$\Delta p_g = (\rho_c - \rho_h) g \Delta Z, \tag{2.08-1}$$

where ρ_c is the cold leg density and ρ_h is the hot leg density.

For the frictional pressure drop, we first assume it is of the form

$$\Delta p_f = f \frac{L}{D_e} \frac{G^2}{2\bar{\rho}}, \tag{2.08-2}$$

where G is the mass flux, $\bar{\rho}$ is the average loop density, D_e is the equivalent loop diameter, and f is the dimensionless friction factor. We know that the general expression for f is

$$f = \frac{C}{Re^n}, \tag{2.08-3}$$

where C and n are constants. For laminar flow, n=1, while for turbulent flow, n approaches zero. Zvirin (Ref.24) has concluded that flow in a PWR system under natural circulation conditions remains turbulent. For turbulent flow in rod bundles, n=.2, so this is the number we will assume for our flow loop. Substituting (2.08-3) into (2.08-2) yields

$$\Delta p_f = \frac{C}{Re^{.2}} \frac{L}{D_e} \frac{G^2}{2\bar{\rho}}.$$

From the definition of Reynolds number,

$$Re = \frac{GD_e}{\mu}. \tag{2.08-4}$$

This can be substituted into (2.08-3) resulting in

$$\Delta p_f = \frac{C}{2} \frac{\mu^{.2} L}{D_e^{1.2}} \frac{G^{1.8}}{\bar{\rho}} \quad . \tag{2.08-5}$$

Recognizing that $\dot{m}_s = GA_c$, where A_c is the cross-sectional area and $\dot{m}_s$ is the flow rate from the upper plenum to the steam generators, we can rewrite (2.08-5) as

$$\Delta p_f = \left[\frac{C}{2} \frac{\mu^{.2} L}{D_e^{1.2} A_c^{1.8}}\right] \frac{\dot{m}_s^{1.8}}{\bar{\rho}} \quad . \tag{2.08-5A}$$

If we assume that the viscosity, μ, is constant for water in the region of interest, then the variables in parenthesis are constant with time and will be lumped together into a constant called R. The final expression for the frictional pressure drop is thus

$$\Delta p_f = \frac{R \dot{m}_s^{1.8}}{\bar{\rho}} \quad . \tag{2.08-6}$$

If we know the full-power flow rate, pressure drop, and average loop density for a given reactor (from FSAR data, for instance), the constant R can be calculated.

Setting the equation for the friction pressure drop equal to the gravity pressure rise and solving for the loop flow, $\dot{m}_s$, we obtain

$$\dot{m}_s = \left[\frac{(\rho_c - \rho_h) g \Delta Z \bar{\rho}}{R}\right]^{1/1.8} \quad . \tag{2.08-7}$$

If we represent the full-power forced convection flow rate as $\dot{m}_{so}$, we can write the following expression for the loop flow $\dot{m}_s$.

$$\dot{m}_s = \begin{cases} \dot{m}_{so} & \text{Forced circulation} \\ \dot{m}_{so} e^{-t/\tau} & \text{Coastdown} \\ \left[\dfrac{(\rho_c - \rho_h) g \Delta Z \bar{\rho}}{R}\right]^{1/1.8} & \text{Natural circulation} \end{cases} \qquad (2.08\text{-}8)$$

For the short period time after a pump trip when both loop coastdown and natural convection are important for determining the correct flow rate, the natural convection and coastdown flow rates are calculated independently and the maximum of the two is used for the loop flow rate, $\dot{m}_s$. Because the time constant of the coastdown is relatively small ($\tau \simeq 16$s typically), this simplification should have little effect on the transient prediction capability of FABREC.

2.9 Steam Generator Secondary Side

FABREC was designed to model a loss-of-all-feedwater transient simultaneous with main steam line isolation. When feedwater is first lost, no mass enters or leaves the steam generator secondaries. Because heat continues to be transferred from the primary, energy is being added but no energy is leaving the node. The result is a pressure increase. Pressure will continue to increase until the setpoint pressure of the atmospheric relief valves is reached. At this point, the valves alternately open and closely maintain the pressure very close to this setpoint pressure.

Remember, the pressure is specified for a Type I node but is calculated for a Type II. Thus, before the relief valves open, we can model this node as a Type II node. After the relief valves open, the pressure is effectively constant. From that point on, we assume the secondary is a Type I node.

Table 2.5 lists what the variables used in the steam generator secondary equations represent. Let us first consider the period of time before the relief valves open. We can write down the energy equation for the entire secondary side of the steam generators

$$\frac{d}{dt}(m_2 u_2) = \dot{Q}_{sg} \quad . \tag{2.09-1}$$

Expanding the left-hand side of (2.09-1) and recognizing that

$$\frac{dm_2}{dt} = 0 \quad , \tag{2.09-2}$$

yields

$$\frac{du_2}{dt} = \frac{\dot{Q}_{sg}}{m_2} \quad . \tag{2.09-3}$$

Now, we know the node-averaged density is constant before the safety valves open because the node is of constant volume and experiences no mass transfer. Thus,

the pressure can be determined from the equation of state

$$p_2 = p(u_2,\rho_2). \qquad (2.09\text{-}4)$$

After the pressure on the secondary side reaches the pressure of the relief valves, we have a Type I node. We can assume the specified pressure is equal to the relief valve setpoint and the inlet flow equals zero. Let us now consider the liquid in the steam generator secondaries as our control volume, as shown in Figure 2-5. The mass, energy, and volume equations become, respectively,

$$\frac{dm_{st}}{dt} = -\dot{m}_b \qquad (2.09\text{-}5)$$

$$\frac{d(m_{st}u_{st})}{dt} = \dot{Q}_{sg} - m_b h_g - p_2 \frac{dV_{st}}{dt} \qquad (2.09\text{-}6)$$

$$\frac{dV_{st}}{dt} = \frac{d}{dt}(m_{st}v_{st}) \quad . \qquad (2.09\text{-}7)$$

Our first simplification is that that liquid in our control volume is at constant, saturated conditions. Substituting saturated liquid properties for our liquid properties after substituting (2.09-5) and (2.09-7) into (2.09-6) yields

$$-u_f\dot{m}_b = \dot{Q}_{sg} - \dot{m}_b h_g + p_2 v_f \dot{m}_b, \qquad (2.09\text{-}8)$$

which can be solved for $\dot{m}_b$, the boiling rate,

$$\dot{m}_b = \frac{\dot{Q}_{sg}}{h_g - u_f - pv_f} \quad . \qquad (2.09\text{-}9)$$

Recognizing that

$$h_f = u_f + p_2 v_f, \qquad (2.09\text{-}10)$$

we can say that

$$\dot{m}_b = \frac{\dot{Q}_{sg}}{h_g - h_f} \; . \qquad (2.09\text{-}11)$$

Equation (2.09-11) is used by FABREC to update the liquid inventory on the secondary side of the steam generator after the relief valves have opened so that the correct primary to secondary heat transfer can be calculated.

2.10 Pressurizer

In FABREC, the pressurizer is a Type II node. The pressure calculated is the specified pressure for the other node representing the primary system. The inlet and outlet flows of the pressurizer node are specified.

The model used for the pressurizer is the simple equilibrium model. This assumes the liquid and steam in the pressurizer are at the same temperature, i.e., are both saturated. This greatly simplifies the calculation of the pressure.

Table 2.6 lists the representation of the variables used in the pressurizer equations. Let's begin the derivation of the pressure by first writing down the mass and energy equations for the entire pressurizer,

$$\frac{d\dot{m}_f}{dt} + \frac{d\dot{m}_g}{dt} = \dot{m}_{up} - \dot{m}_{srv} - \dot{m}_{porv} \tag{2.10-1}$$

$$\frac{d}{dt}(m_f u_f) + \frac{d}{dt}(m_g u_g) = \dot{m}_{up} h_{up} - \dot{m}_{srv} h_{srv} - \dot{m}_{porv} h_{porv}. \tag{2.10-2}$$

Our pressurizer is of constant volume so that

$$\frac{d}{dt}(m_f v_f) + \frac{d}{dt}(m_g v_g) = 0. \tag{2.10-3}$$

Expanding the left-hand sides of (2.10-2) and (2.10-3) yields

$$\dot{m}_f u_f + m_f \dot{u}_f + \dot{m}_g u_g + m_g \dot{u}_g = \dot{m}_{up} h_{up} - \dot{m}_{srv} h_{srv} - \dot{m}_{porv} h_{porv} \tag{2.10-4}$$

$$\dot{m}_f v_f + m_f \dot{v}_f + \dot{m}_g v_g + m_g \dot{v}_g = 0. \tag{2.10-5}$$

The reader might have noticed that the variable for which we wish to solve, p, does not appear in the above equations. We introduce the pressure into our equations from the observation that the liquid and steam properties, because they are saturated, can be written as

$$u_f = u_f(p), \tag{2.10-6}$$

$$u_g = u_g(p), \tag{2.10-7}$$

$$v_f = v_f(p), \tag{2.10-8}$$

$$v_g = v_g(p). \tag{2.10-9}$$

Differentiating both sides of the above equations with respect to time results in

$$\dot{u}_f = \frac{du_f}{dp}\,\dot{p}, \tag{2.10-10}$$

$$\dot{u}_g = \frac{du_g}{dp}\,\dot{p}, \tag{2.10-11}$$

$$\dot{v}_f = \frac{dv_f}{dp}\,\dot{p}, \tag{2.10-12}$$

$$\dot{v}_g = \frac{dv_g}{dp}\,\dot{p}. \tag{2.10-13}$$

The derivation of the rate of change of pressure, $\dot{p}$, from these equations is a long and tedious procedure. Those interested can refer to the Appendix. We will only present the result here.

$$\dot{p} = \frac{\begin{array}{l}\dot{m}_{up}h_{up}-\dot{m}_{porv}h_{porv}-\dot{m}_{srv}h_{srv}+u_f(\dot{m}_{porv}+\dot{m}_{srv}-\dot{m}_{up}) \\ +(\dot{m}_{up}-\dot{m}_{porv}-\dot{m}_{srv})\left(\frac{v_f}{v_g-v_f}\right)(u_g-u_f)\end{array}}{m_f\left(\frac{du_f}{dp}\right)+m_g\left(\frac{du_g}{dp}\right)-\left(\frac{dv_f}{dp}\right)\left(\frac{m_fu_g-m_fu_f}{v_g-v_f}\right)-\left(\frac{dv_g}{dp}\right)\left(\frac{m_gu_g-u_f}{v_g-v_f}\right)} \tag{2.10-14}$$

$$\dot{m}_g = \frac{-m_f\left(\frac{dv_f}{dp}\right)\dot{p} - \dot{m}_{up}v_f + (\dot{m}_{porv} + \dot{m}_{srv})v_f - m_g\left(\frac{dv_g}{dp}\right)\dot{p}}{v_g - v_f} \qquad (2.10\text{-}15)$$

$$\dot{m}_f = \dot{m}_{up} - \dot{m}_{porv} - \dot{m}_{srv} - \dot{m}_g \qquad (2.10\text{-}16)$$

Because the entire pressurizer is modeled to be in thermal equilibrium, cold insurges may actually lower the pressure. This is because the insurge would lower the node-average internal energy. To correct for this, when there is an insurge, $\dot{m}_{up}$, that is subcooled with enthalpy h_{up}, the insurge enthalpy is adjusted to a new value which is the arithmetic average of the insurge and saturated fluid enthalpies. This adjustment produces increasing pressurizer pressure with subcooled insurges, which is physically correct.

As of yet, it was not mentioned how to obtain the flow or enthalpy discharged out the valves. As was stated previously, FABREC assumes instanteous phase separation in the pressurizer. The PORVs and SRVs are connected to the top of the pressurizer, so the assumption is that the flow exiting the pressurizer is liquid only if there is no steam in the pressurizer. Otherwise, the flow out the valves is saturated steam. In other words,

$$h_{srv} = h_{porv} = \begin{cases} h_f & \text{if } m_g = 0 \\ h_g & \text{if } m_g \neq 0. \end{cases} \qquad (2.10\text{-}17)$$

For the flow out the valves, different correlations are used for liquid or steam upstream conditions. In both cases though, the flow is assumed to be critical, or choked. In general, the liquid choked flow rate is greater than that of the steam.

For liquid entering the valve, FABREC uses the Burnell correlation to predict the critical flow. This is a closed form equation based on a homogeneous, non-equilibrium flow model. The correlation is

$$G = \sqrt{2\rho_\ell g_c[p_o-(1-C)p_{sat}(T_o)]}, \qquad (2.10\text{-}18)$$

$$C = \frac{0.294\ \sigma\ (T_o)}{\sigma(p_{sat}=175\text{psia})},$$

where G is the mass flux, σ is the surface tension, and p_o and T_o are the liquid pressure and temperature.

For steam upstream of the valves, Napier's formula is used with the Thompson and Buxton correction factor. These equations are

$$G = \frac{p_o}{70} K_n \qquad (2.10\text{-}20)$$

$$K_n = \frac{0.1906p_o-1000}{0.2292p_o-1061} \quad 1500<p_o<3200\text{psia}. \qquad (2.10\text{-}21)$$

Discharge coefficients and recommended choking areas were obtained from Ref.5 for both liquid and steam upstream conditions. These values are the result of the EPRI Safety and Relief Valve Test Program. For more information on the critical flow models and testing procedures, the reader should consult Ref.1.

2.11 Core Heat Generation

After shutdown, FABREC calculates the decay heat rate as a function of time. The decay heat curve is based on the 1979 ANS-5.1 Standard for Thermal Fission of U-235 with an Infinite Operating History (Ref.3). A correction factor of 1.02 is added to account for the decay of fission products other than those from U-235. The decay power curve is

$$\frac{\dot{Q}_c}{Q_{co}} = \begin{cases} (1.02)(\frac{12.4358}{200})t_d^{-0.102867} & 0<t_d\leq 6 \\ (1.02)(\frac{14.0960}{200})t_d^{-0.171702} & 6<t_d\leq 40 \\ (1.02)(\frac{16.0951}{200})t_d^{-0.207240} & 40<t_d\leq 200 \\ (1.02)(\frac{19.4829}{200})t_d^{-.2374004} & 200<t_d\leq 1500 \\ (1.02)(\frac{30.9998}{200})t_d^{-.302264} & t_d>1500, \end{cases} \qquad (2.11\text{-}1)$$

where t_d is the time after shutdown in seconds and a value of 200 MeV/fission is used.

2.12 Emergency Core Cooling System

The ECCS has as its suction the refueling water tank (RWT) and discharges into the cold legs of the reactor coolant system. The RWT is a large tank at atmospheric pressure. The main components of ECCS are the ECC water pumps.

The injection flow , $\dot{m}_{i\ell}$, is calculated from the head-flow curves characteristic of the pumps. The head developed is equal to the pressure difference between the primary system and the RWT. Gravity and kinetic energy are neglected.

In order to calculate the enthalpy of the ECC water entering the RCS, we first write down a differential equation for the enthalpy for a pure substance,

$$dh = vdp+Tds \quad . \tag{2.12-1}$$

If we assume the pumping is isentropic (adiabatic and reversible), we can write

$$dh = vdp \quad . \tag{2.12-2}$$

Also, for subcooled water, it is nearly incompressible so that

$$\Delta h = v\Delta p \quad . \tag{2.12-3}$$

Substituting for Δh and Δp, we obtain

$$h_{i\ell}-h_{tank} = v(p-p_a), \tag{2.12-4}$$

where $h_{i\ell}$ and h_{tank} are the ECC and RWT water enthalpies, respectively, p is the primary pressure, and p_a is atmospheric pressure. Solving for $h_{i\ell}$ yields

$$h_{i\ell} = h_{tank} + v(p-p_a) \tag{2.12-5}$$

(2.12-5) is used to calculate the enthalpy of the ECC water injected.

2.13 Description of Code

The general flowchart of FABREC is shown in Figure 2-6. Subroutines INIT and GEOM read the input data and set the remaining system variables such that the PWR is at steady-state. For instance, the upper and lower plenum temperatures and loop flow are input by the user. From this information, an energy balance is performed on the core to calculate the core power specified by these temperatures and flows. The primary-to-secondary heat transfer rate is set equal to the core power and the steady-state steam generator heat transfer coefficient is calculated. The result is that the system variables necessary for steady-state operation are calculated non-iteratively.

After the steady-state calculation is made, FABREC begins the first transient pass. One pass is made for each time step since the integration is fully explicit. Subroutine ECCS first determines the ECC flow and enthalpies. Subroutines STMGEN, LPL, CORE, UPL, and PRESS update the conditions in the steam generator primaries, lower plenum, core, upper plenum, and pressurizer, respectively. In addition, subroutine VALVE calculates the PORV and SRV flow rates. Function GENMASS updates the water inventory on the steam generator secondaries and function QC determines the core (decay) power.

After this pass, the time is updated. The next time step size is also calculated. The conditions for stopping the transient calculation are tested (for example, if time exceeds a pre-determined valve), and if satisfied, the transient calculation ends. If not, another pass is initiated.

Thermodynamic properties of water used by FABREC are all calculated by function subprograms. Some of these functions were fitted from steam tables (Ref.7) and others are identical to those used by TRAC (Ref.8). These functions calculate the properties with pressure and temperature as their independent variables.

A detailed description of FABREC and its input will be contained in a forthcoming BNL report.

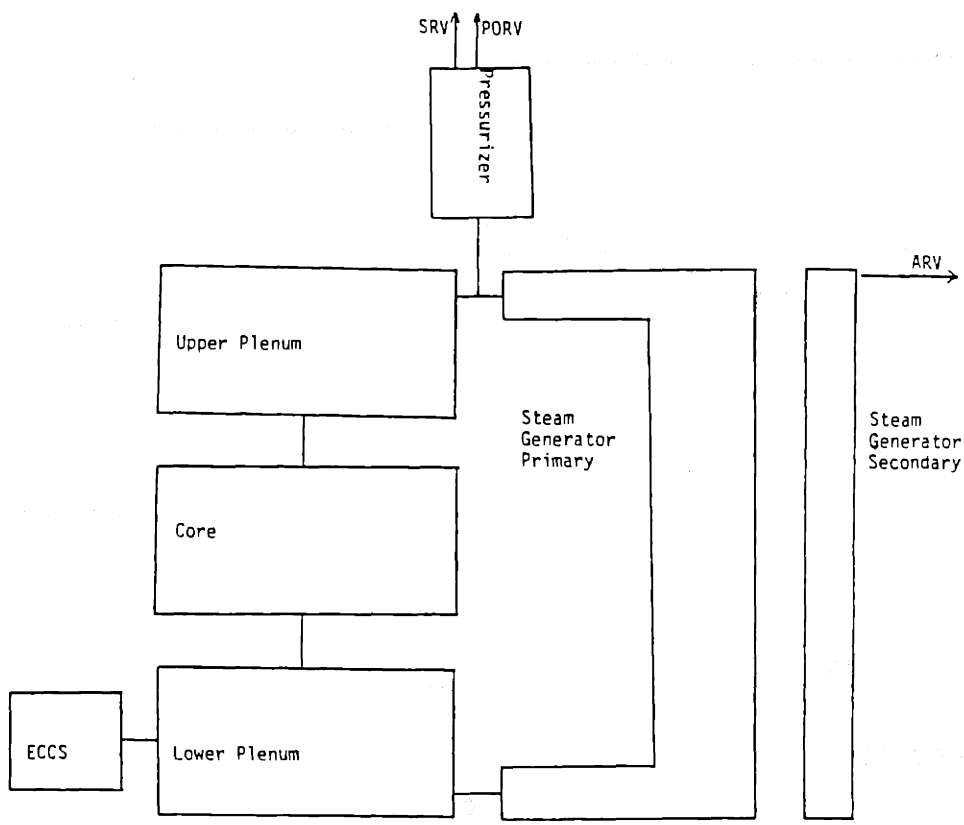

Figure 2-1 FABREC noding scheme.

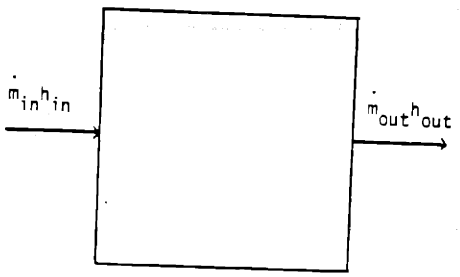

Figure 2-2 Control volume for Type I (pressure specified) node.

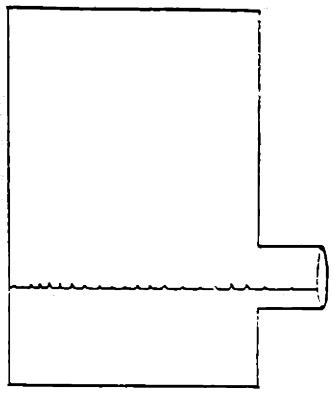

Figure 2-3 FABREC representation of the upper plenum. The fluid leaving the plenum out the nozzle is liquid until the mixture level reaches the top of the nozzle.

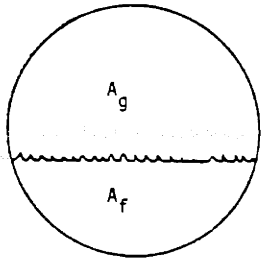

Figure 2-4 Cross-section of the nozzle. The flow is assumed to be homogeneous with a void fraction equal to the area occupied by the steam divided by the total nozzle cross-sectional area.

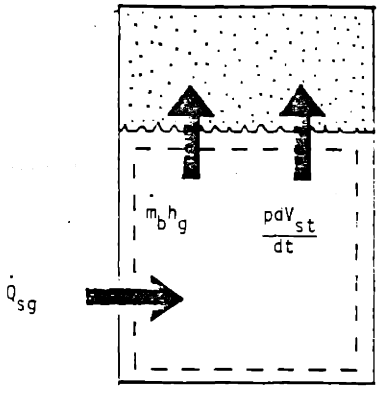

Figure 2-5 Control volume for the liquid in the steam generator secondaries.

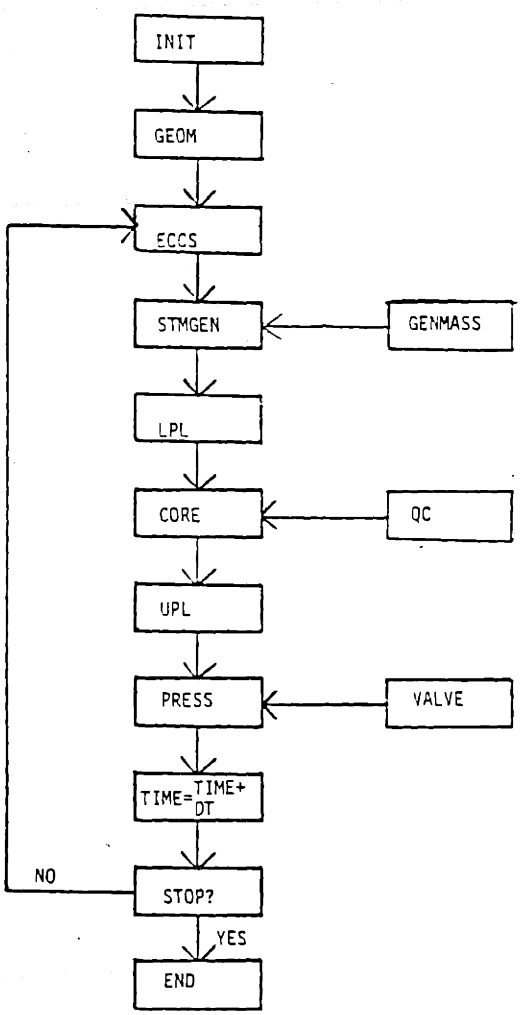

Figure 2-6 Flowchart of FABREC showing principal subroutines and functions.

Table 2.1 Variables Used in Lower Plenum Equations

$\dot{m}_{i\ell}$	ECC injection flow
$\dot{m}_{s\ell}$	Flow from steam generator to lower plenum
$\dot{m}_{\ell c}$	Flow from lower plenum to core
m_ℓ	Mass of lower plenum fluid
$h_{i\ell}$	Enthalpy of $\dot{m}_{i\ell}$
$h_{s\ell}$	Enthalpy of $\dot{m}_{s\ell}$
$h_{\ell c}$	Enthalpy of $\dot{m}_{\ell c}$
h_ℓ	Node-averaged enthalpy of lower plenum fluid
ρ_ℓ	Node-averaged density of lower plenum fluid
V_ℓ	Volume of lower plenum fluid

Table 2.2 Variables Used in Core Equations

$\dot{m}_{\ell c}$	Flow from lower plenum to core
$\dot{m}_{cu}$	Flow from core to upper plenum
m_c	Mass of core fluid
$h_{\ell c}$	Enthalpy of $\dot{m}_{\ell c}$
h_{cu}	Enthalpy of $\dot{m}_{cu}$
h_c	Node-averaged enthalpy of core fluid
ρ_c	Node-averaged density of core fluid
V_c	Volume of core fluid
$\dot{Q}_c$	Core power

Table 2.3 Variables Used in Upper Plenum Equations

$\dot{m}_{cu}$	Flow from core to upper plenum
$\dot{m}_{us}$	Flow exiting upper plenum
m_u	Mass of upper plenum fluid
h_{cu}	Enthalpy of $\dot{m}_{cu}$
h_{us}	Enthalpy of $\dot{m}_{us}$
h_u	Node-averaged enthalpy of upper plenum fluid
h_f	Saturated fluid enthalpy
h_g	Saturated vapor enthalpy
ρ_u	Node-averaged density of upper plenum fluid
ρ_f	Saturated fluid density
ρ_g	Saturated vapor density
V_u	Volume of upper plenum fluid
A_g	Cross sectional area of steam in outlet nozzle
A_f	Cross sectional area of fluid in outlet nozzle
A_n	Cross sectional area of nozzle
α	Void fraction of nozzle flow

Table 2.4 Variables Used in Steam Generator Primary Equations

$\dot{m}_s$	Flow to steam generator
$\dot{m}_{s\ell}$	Flow exiting steam generators
m_{st1}	Mass of fluid in primary piping and steam generators
h_s	Enthalpy of $\dot{m}_{s\ell}$
h_{us}	Enthalpy of $\dot{m}_s$
V_s	Volume of m_{st1}
$\dot{Q}_{sg}$	Primary-to-secondary heat transfer rate

Table 2.5 Variables Used in Steam Generator Secondary Equations

$\dot{m}_b$	Rate of boiling on steam generator secondary
m_{st}	Mass of liquid in steam generator secondary
m_2	Mass of fluid in steam generator secondary
u_2	Average internal energy of fluid in steam generator secondary
p_2	Pressure of steam generator secondary
u_{st}	Internal energy of liquid in steam generator secondary
u_f	Internal energy of saturated liquid
h_g	Enthalpy of saturated liquid
v_f	Specific volume of saturated liquid
v_{st}	Specific volume of steam generator secondary liquid
$\dot{Q}_{sg}$	Primary-to-secondary heat transfer rate
V_{st}	Volume of steam generator secondary liquid

Table 2.6 Variables Used in Pressurizer Equations

Subscripts		Variables	
f	Saturated fluid	m	Mass
g	Saturated Vapor	h	Enthalpy
up	Surge	u	Internal energy
porv	PORV	v	Specific volume
srv	SRV	p	Pressure

Section 3

FEED AND BLEED TRANSIENT ANALYSIS

3.1 Introduction

Two transients were chosen for the feed and bleed transient analysis and FABREC verification. In the first, offsite power is lost at the start of the transient. This is followed by a reactor scram and turbine trip. Normally, the auxiliary feedwater pumps would be started since the main feedwater pumps would be unavailable (whether they be turbine or motor-driven). FABREC assumes auxiliary feedwater is unavailable. In this scenario, ECC water is also assumed to be unavailable. After the steam generators boil dry, there is no heat sink for the primary system, which is being heated by decay heat, and thus, this sequence leads to a core melt.

In the second transient, again the auxiliary feedwater is not available; however, at ten minutes into the transient, the operator manually initiates a safety injection. The PORV setpoint, which can be changed from the control room by the operator, is assumed to be unaltered. This is in contrast to some "bleed and feed" procedures in which the operator either lowers the setpoint of the PORVs or latches them open. This would be necessary in plants in which the ECC flow is insufficient at the operating PORV setpoint (which is the case in most Combustion Engineering plants). Thus, our scenario would be typical of plants that have safety-grade charging (make-up) flow. For successful feed and bleed at the PORV setpoint pressure, the capacities of both the PORVs and the ECCS must be sufficient to cool the core. Figure 3-0 shows qualitatively how the capacities of the PORVs and ECCs relate to the core decay power, for an injection rate of $\dot{m}_{i\ell}$ and PORV capacity of $\dot{m}_{porv}$. As can be seen in the figure, the ECCS capacity will determine if the feed and bleed is successful.

The plant chosen to analyze was Zion 1, owned and operated by Commonwealth Edison. This is a four-loop Westinghouse PWR. Safety-grade

make-up flow is from two centrifugal charging pumps (CCPs). Although these pumps are part of the chemical and volume control system (CVCS), normal charging during steady-state operation is accomplished by a positive displacement pump (PDP), which is not safety-grade. The source of the ECC water is the refueling water tank (RWT). When the water level in this tank falls below some pre-determined value, the RWT is isolated and the ECC pumps take suction from the water in the containment sump. No analysis was performed on this "recirculation" mode of core cooling.

The PORVs and SRVs were modeled as variable opening valves. The valves start to open at their corresponding setpoint pressure and are fully open at 0.1 MPa above their setpoint. As a result, the valves do not flutter open and closed, but rather tend to sit at some partially open position. Because the valves do not flutter, a large time step can be used. Thus, the stability and economy of FABREC is increased by the choice of this valve model.

3.2 Case 1 - ECCS Unavailable

Table 3.1 shows the event sequence for this transient. The initiating event for this transient was assumed to be a loss of offsite power event. This would trip the turbines, reactor coolant pumps, main feedwater pumps, and generate a scram signal. Under normal circumstances, this transient would end by starting the auxiliary feedwater pumps, which would replenish the water inventory of the steam generators boiled off by the core decay heat. FABREC assumes auxiliary feedwater is unavailable.

Figure 3-1 shows the decay power as a function of time. After the scram, the power rapidly falls off from its initial value of 3188 MW. The decay heat generated is approximately proportional to time raised to the negative one-fifth power. Because the decay heat is not from fission, but rather from the decay of fission products, it is dependent only on time.

The heat sink for this transient is the water initially present in the steam generators. As this water is boiled off, heat transfer from the primary to the secondary is degraded. Figure 3-2 shows how the liquid water inventory of steam generators decreases with time. The initial inventory is approximately 1.62×10^5 kg. Very little heat sink remains 80 minutes into the transient.

After the reactor coolant pumps are tripped at the start of the transient, the loop flow begins a coastdown, as shown in Figure 3-3. After the coastdown, natural circulation is established. The natural circulation flow is approximately 540 kg/s, or about 3% of the full power flow. After about 2 h, the primary system has voided sufficiently to end the natural circulation.

Figure 3-4 shows how the primary temperature varies with time. After the reactor coolant trip, there is an initial rise in temperature caused by the flow coastdown. This is sometimes called a "power-to-flow mismatch". As the temperature rises in the hot leg, the natural circulation flow increases. Also, the higher primary temperature will increase the primary-to-secondary heat transfer. From 10 min to about 75 min, the primary experiences a quasi-steady state condition where the

flow, driven by natural circulation, removes the decay heat from the core and transfers the heat to the water on the secondary side of the steam generator. At about 75 min, the steam generator heat transfer, degraded by the decreased water inventory, is insufficient to balance the decay power of the core. The result is a rise in primary temperatures until the upper plenum saturates at approximately 114 min. After the primary saturates, the vessel inventory removes the decay heat by boiling. Figure 3-5 shows the vessel mixture level decreasing after voiding begins at 114 min. The discontinuity in the slope of the curve at about 122 min occurs because at that point the mixture level reaches the height of the outlet nozzles in the upper plenum. At about 128 min, the core has completely voided. Remember, FABREC models the two-phase flow in the core as one-dimensional homogeneous flow. FABREC cannot model counter-current flow in the upper plenum region. If counter-current flow were to occur, liquid would travel down from the upper plenum to the core. Since FABREC predicts the core will completely void before the upper plenum does, counter-current flow would lengthen the time for the core to uncover.

Figures 3-6 and 3-7 illustrate the pressurizer level and pressure, respectively. There is an initial surge into the pressurizer, caused by the power-to-flow mismatch, which also results in a small pressure rise. From 10 min to 75 min, the pressure and level slowly decreases as decay power is also decreasing, lowering the primary temperature slowly and causing the liquid to contract. After steam generator heat transfer is degraded at 75 min, there is a surge into the pressurizer, raising its level and pressure. The pressurizer PORVs start to open at 16.1 MPa, and the pressurizer goes solid at 100 min. The capacity of the PORVs is sufficient to relieve the volumetric expansion of the primary while it is subcooled; however, when the primary saturates at 114 min, the PORV capacity is no longer able to relieve the volumetric expansion of the primary fluid. The result is a pressure rise to the SRV setpoint of 17.13 MPa, which is reach at 119 min. Up to this time, the flow from the upper plenum to the pressurizer has been liquid since the vessel mixture level has been above the outlet nozzle. As the level moves down past the nozzle at 123 min, steam leaves the plenum, and since it carries away more energy than liquid, we see a pressure drop. A rapid pressure spike follows. The

initial rise is from the rapid boiling of the water left in the vessel. After this water has boiled, little water is left in the core and thus the volumetric expansion of the fluid is mostly due to the thermal expansion of the steam present. Since this is small compared to the combined SRV/PORV capacity, there is a rapid decrease in pressure, followed by complete dryout of the core at 128 min.

Los Alamos has simulated several loss-of-feedwater transients for Zion 1 using the Transient Reactor Analysis Code (TRAC-PD2) (Ref.8). A comparison between TRAC results and those of FABREC for the average core liquid temperature can be seen in Figure 3-8. The general features of the curves are very similar. TRAC predicts a shorter time for the steam generators to dryout. Although the TRAC steam generator dries out earlier, there is only a 6 min difference between the TRAC and FABREC calculation for the time it takes for the primary fluid to saturate (108 and 114 min, respectively). On the secondary side, the codes predict similar values for the secondary pressure (Figure 3-4). The differences between TRAC and FABREC calculations are mainly due to differences in modeling the steam generators. Due to the earlier dryout time on the TRAC calculation, it is believed that there is more water inventory in contact with the primary tubes in the FABREC steam generator model than in that for TRAC. FABREC assumes the entire secondary water inventory is in contact with the tubes, and thus dryout will not occur until all the water has been depleted.

3.3 Case 2 - ECC Injection at Ten Minutes

Table 3.2 lists the sequence of events for this transient. The results are identical to Case 1 until the operator initiates the safety injection at 10 min into the transient (begins the feed and bleed). At that time ECC water is injected into the cold legs of the reactor coolant system and bled out the PORVs.

Figures 3-10 and 3-11 show how the level and pressure in the pressurizer respond to the transient. Initially, there is an insurge due to the power-to-flow mismatch. At 10 minutes, the safety injection is initiated, as shown in Figure 3-13, and causes a rising level in the pressurizer, also leading to a rising pressure. At 18 min, the pressure has reached 16.1 MPa, and the PORVs begin to open. The pressurizer is solid at 25 min and remained in that condition for the rest of the transient. Once the pressure reached the setpoint of the PORVs, the ECCS flow remains almost constant at 12 kg/s. The PORV capacity is more than sufficient to remove the decay power produced by the core, and thus the primary system is never subjected to a pressure rise once the PORVs begin to open.

The steam generators dryout at a much later time with safety injection at 10 min than without safety injection (Figure 3-13). This is because once feed and bleed is started, the steam generators remove only a fraction of the decay heat produced by the core. The remaining fraction of the heat is removed by the ECC water entering the core and leaving out the PORVs. The steam generators now dryout at about 145 min.

There is an initial rise in the primary water temperature caused by the power-to-flow mismatch (Figure 3-14). After the safety injection at 10 min, the primary reaches a state of quasi-steady cooling, until about 125 min, at which time the primary-to-secondary heat transfer has degraded sufficiently to cause a temperature rise in the primary. Although the ECC water continues to remove decay heat from the core, the flow of 12 kg/s is insufficient to maintain subcooling in the upper plenum. The temperature continues to rise until the primary water saturates at 219 min. At this time the decay power is 28.6 MW and the energy is being removed by the ECC

flow at a rate of 29 MW, and therefore, the calculation is ended. Recovery will occur because the decay power is at a level that is removable by the ECC flow.

A comparison of the core temperature cacluated in TRAC and FABREC can be seen in Figure 3-15. TRAC predicts a shorter steam generator dryout time and thus the primary saturates earlier than in the FABREC calculation (192 min compared to 219 min). Again, the reason for the earlier dryout in the TRAC simulation is due to steam generator modeling differences. Both codes predict that recovery will occur once the primary saturates.

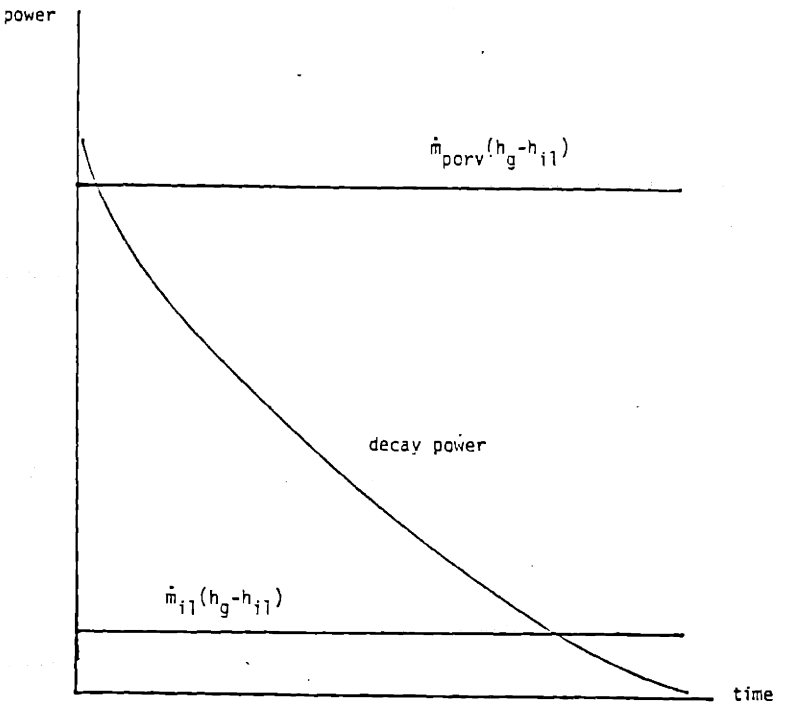

Figure 3-0. Qualitative comparison of the core decay power with the PORV capacity and the ECCS capacity.

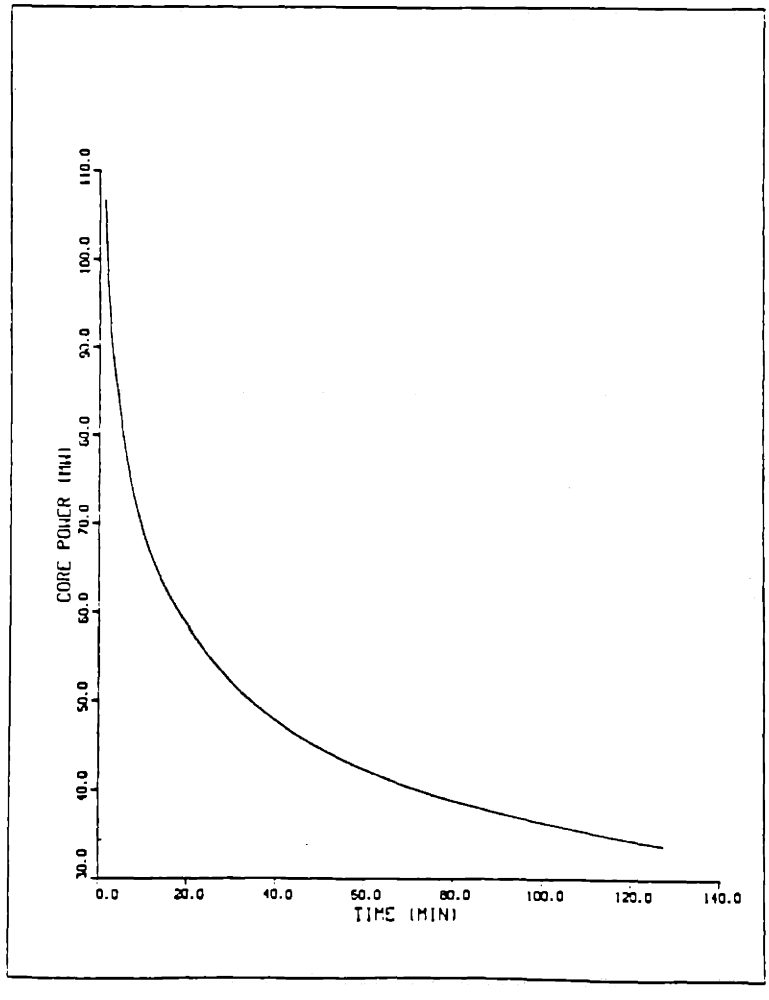

Figure 3-1 After the reactor has scrammed, the power rapidly falls off from its initial value of 3188 MW.

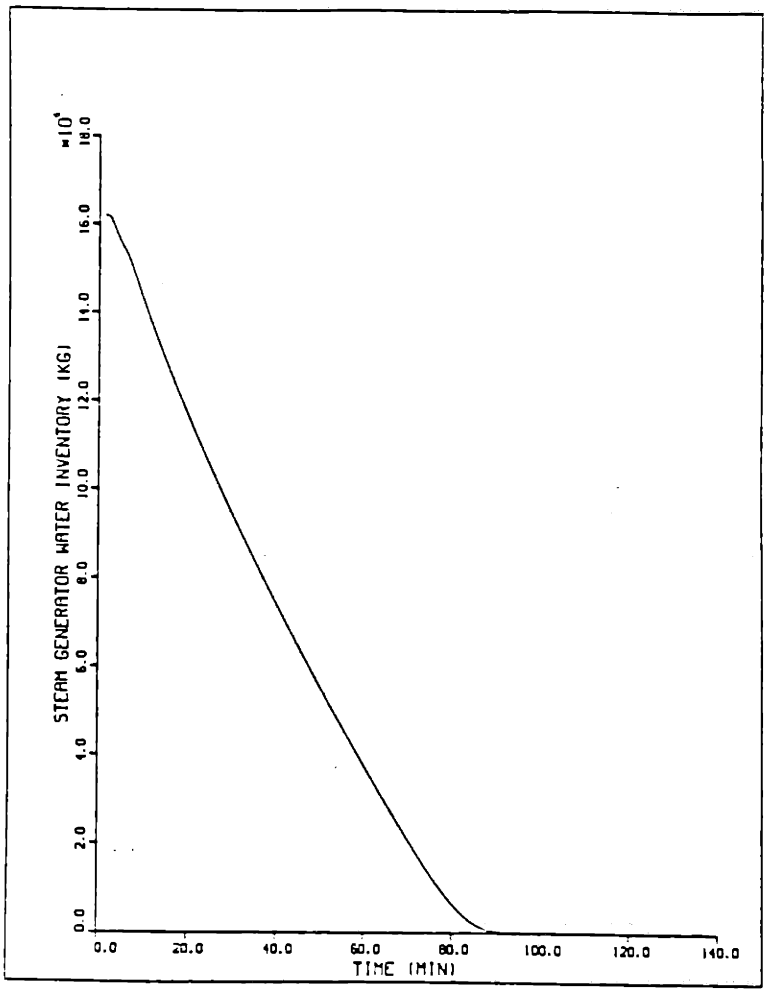

Figure 3-2 The water inventory in the secondaries is depleted soon after 80 min with no auxiliary feedwater available.

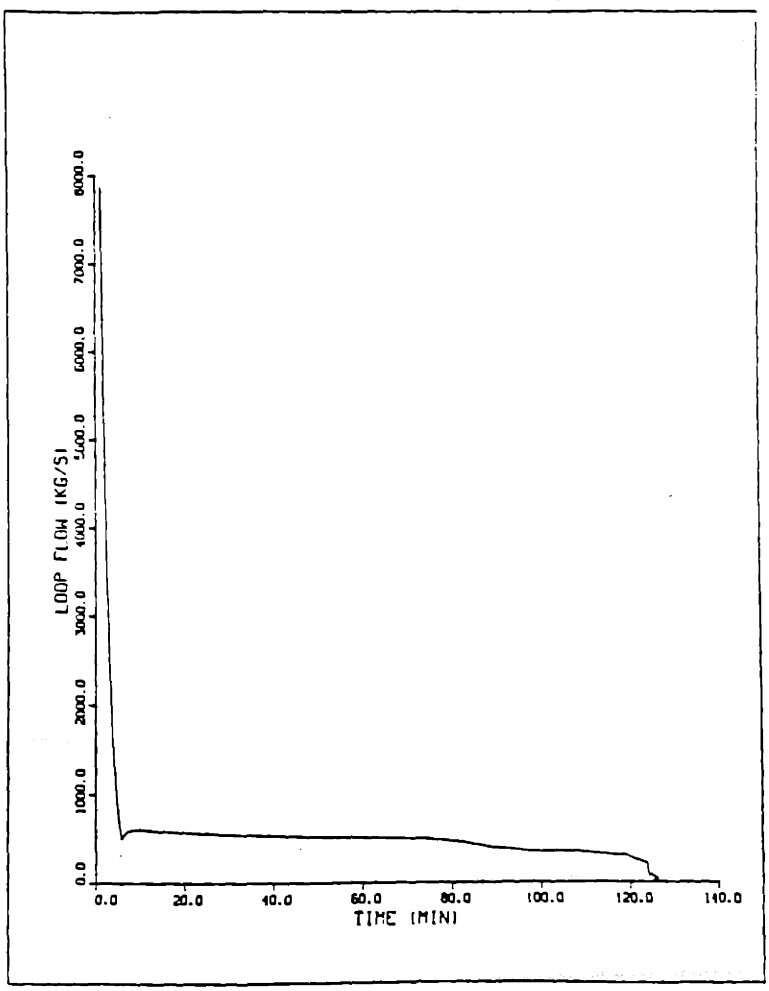

Figure 3-3 The natural circulation ends when the primary has sufficiently voided after about 2 h.

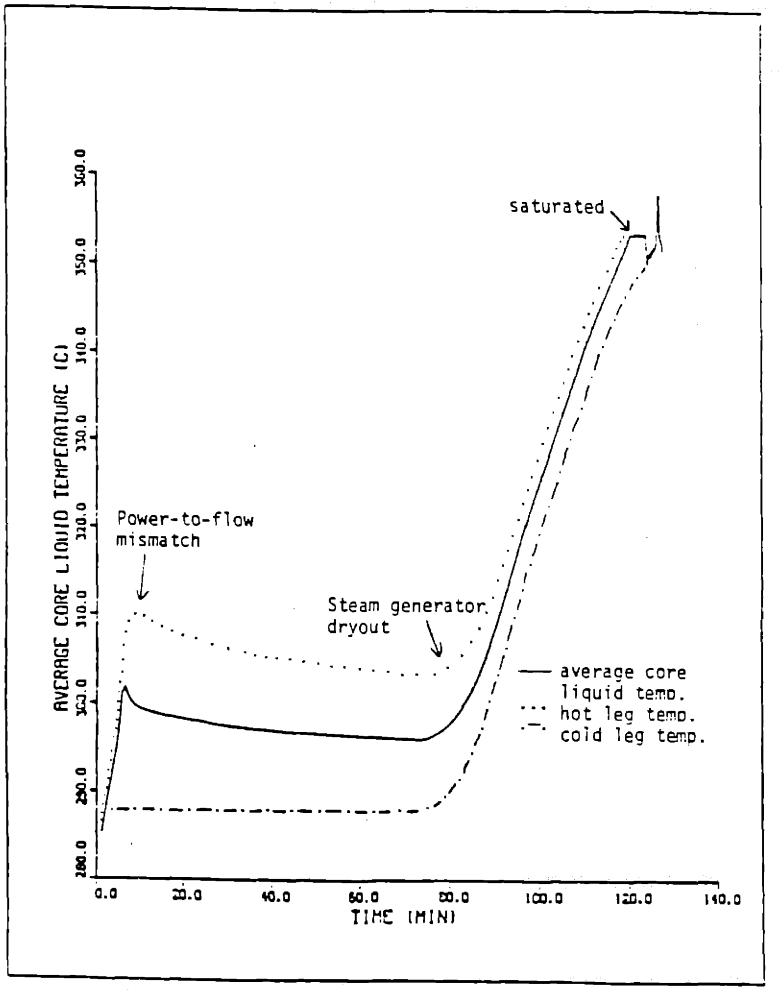

Figure 3-4 There is a sharp rise in the primary temperatures after the primary to secondary heat transfer is degraded at 75 min.

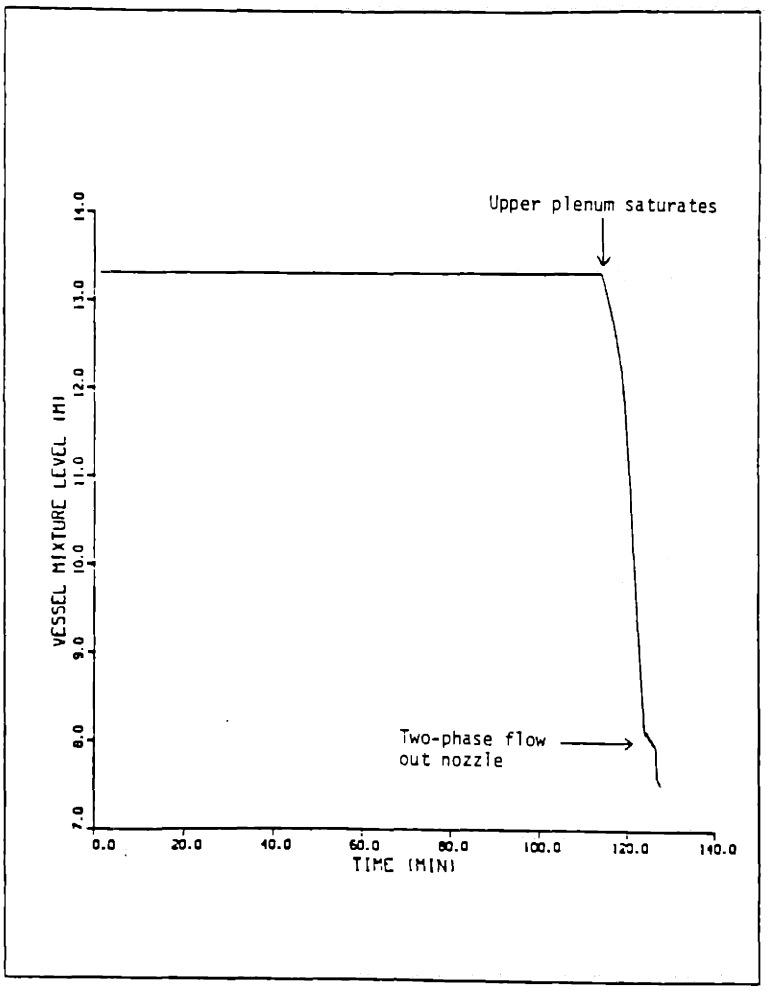

Figure 3-5 The vessel mixture level decreases after voiding begins at 114 min.

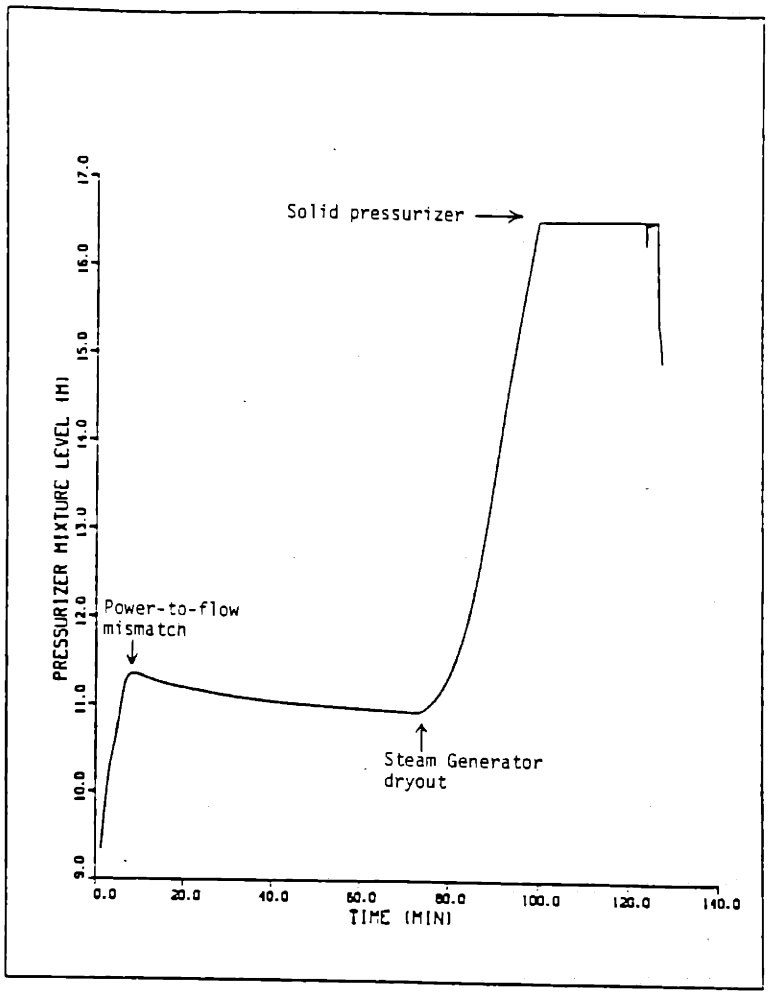

Figure 3-6 After dryout, the pressurizer goes solid.

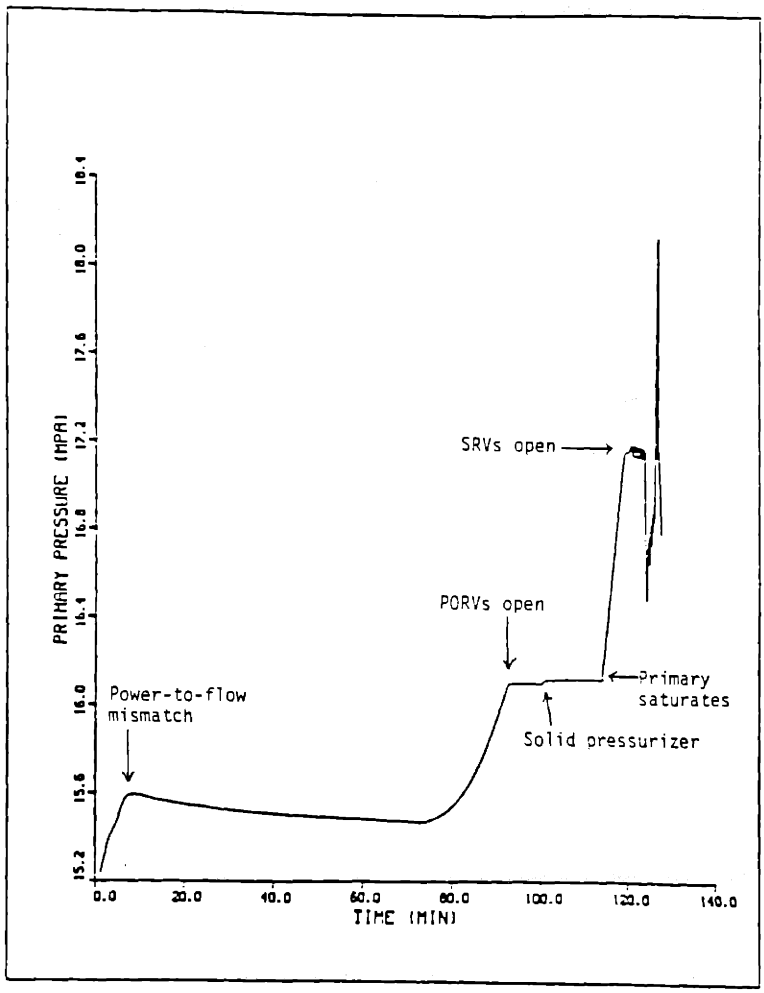

Figure 3-7 Primary pressure when there is no ECC injection.

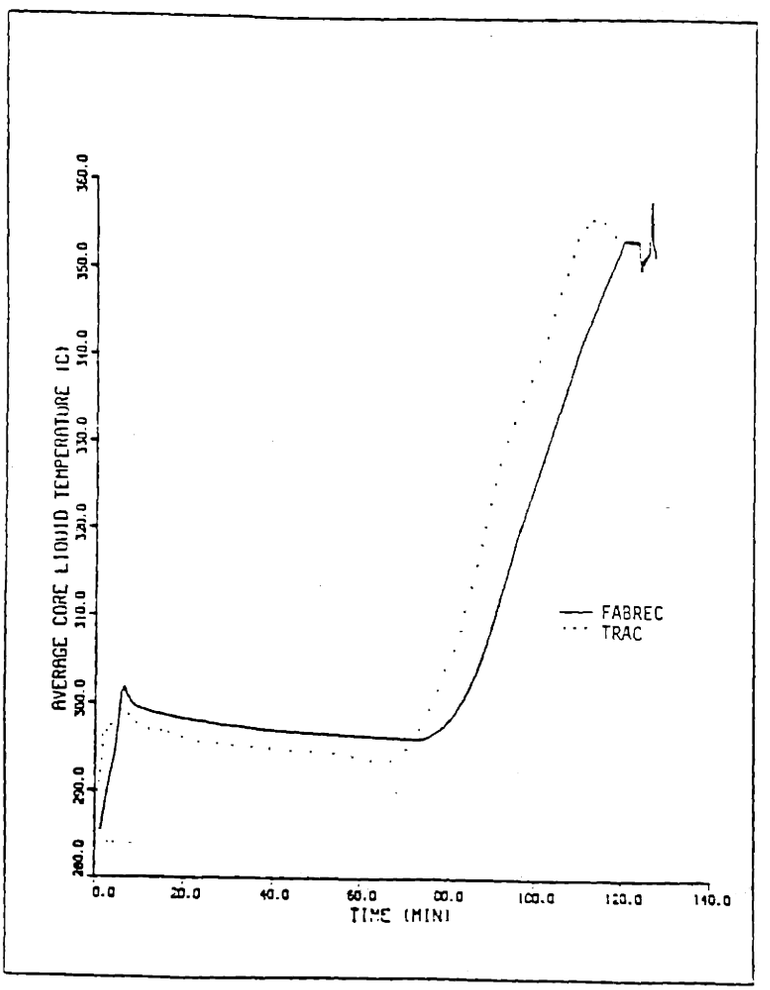

Figure 3-8 Comparison of TRAC and FABREC core temperature calculations.

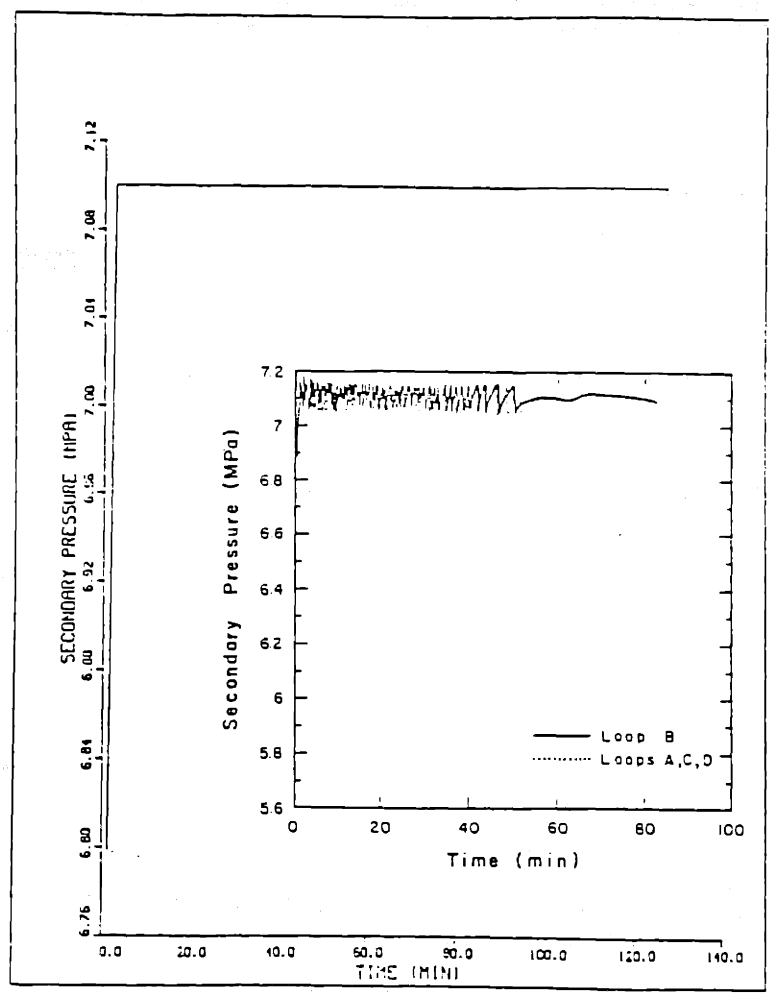

Figure 3-9 Comparison of steam generator secondary pressure as calculated in FABREC (outer graph) and TRAC (inset).

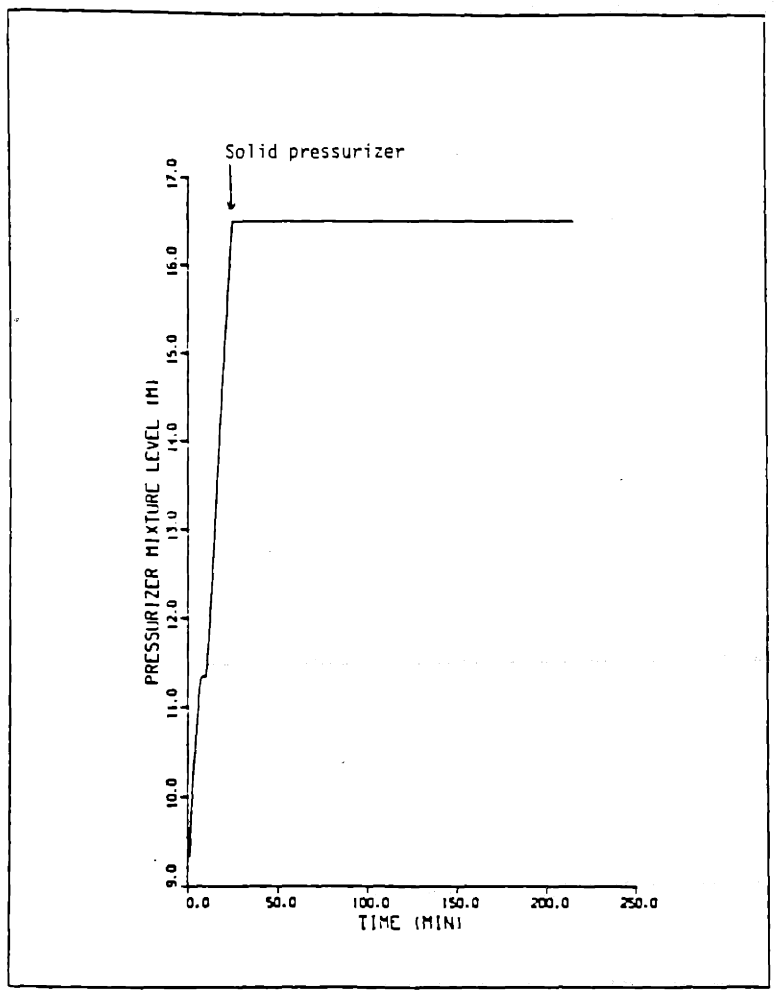

Figure 3-10 The pressurizer goes solid at 25 min when ECC is initiated at 10 min.

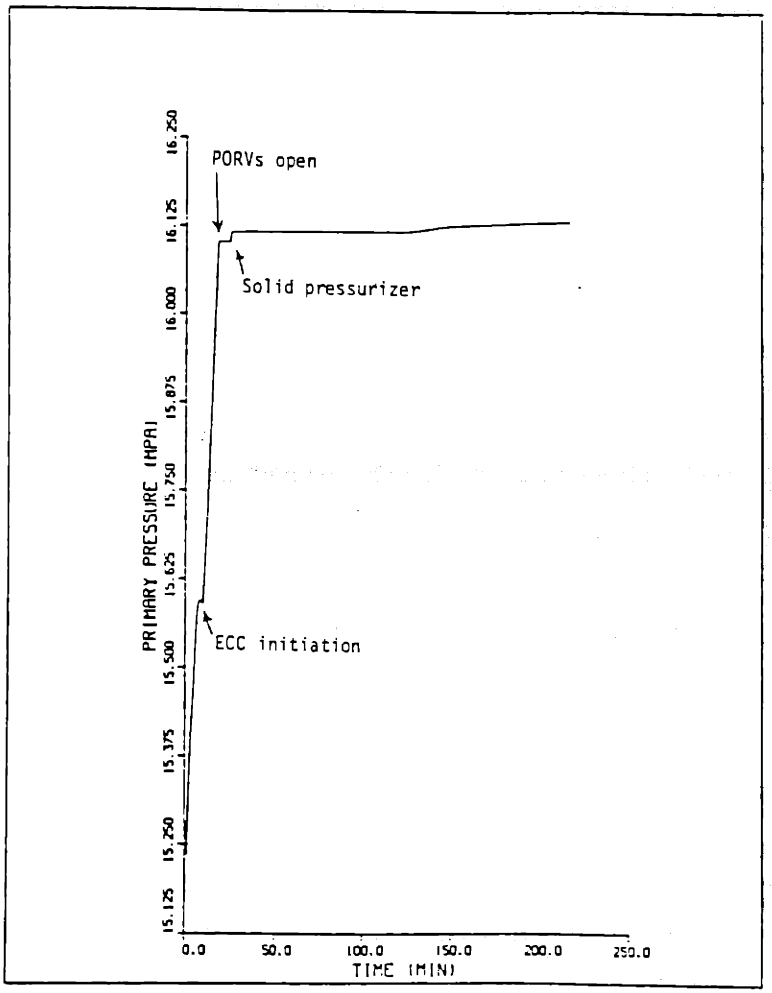

Figure 3-11 Primary pressure increases to PORV setpoint and remains there while primary is subcooled.

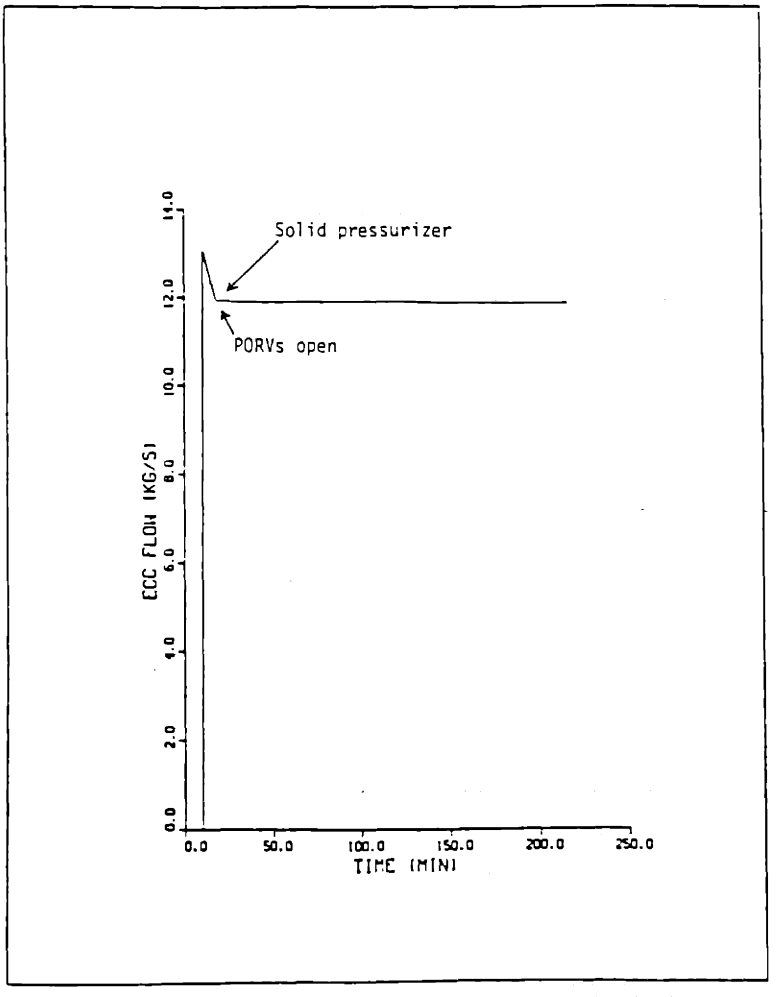

Figure 3-12 Safety injection is initiated manually at 10 min.

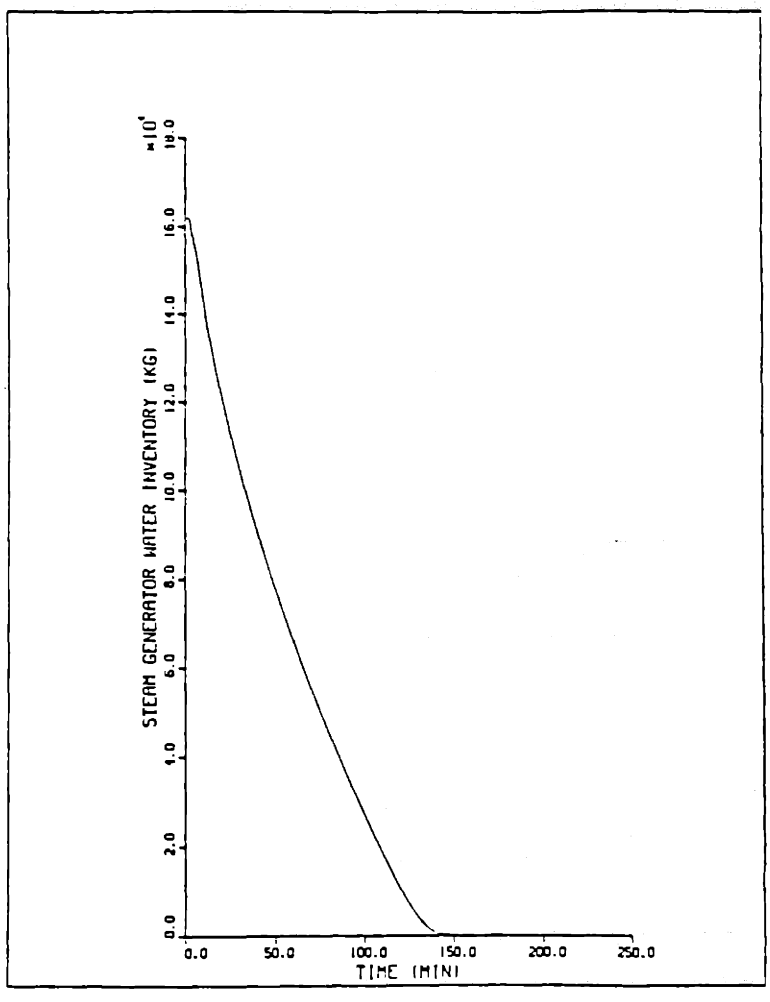

Figure 3-13 The steam generators have little water inventory after 145 min.

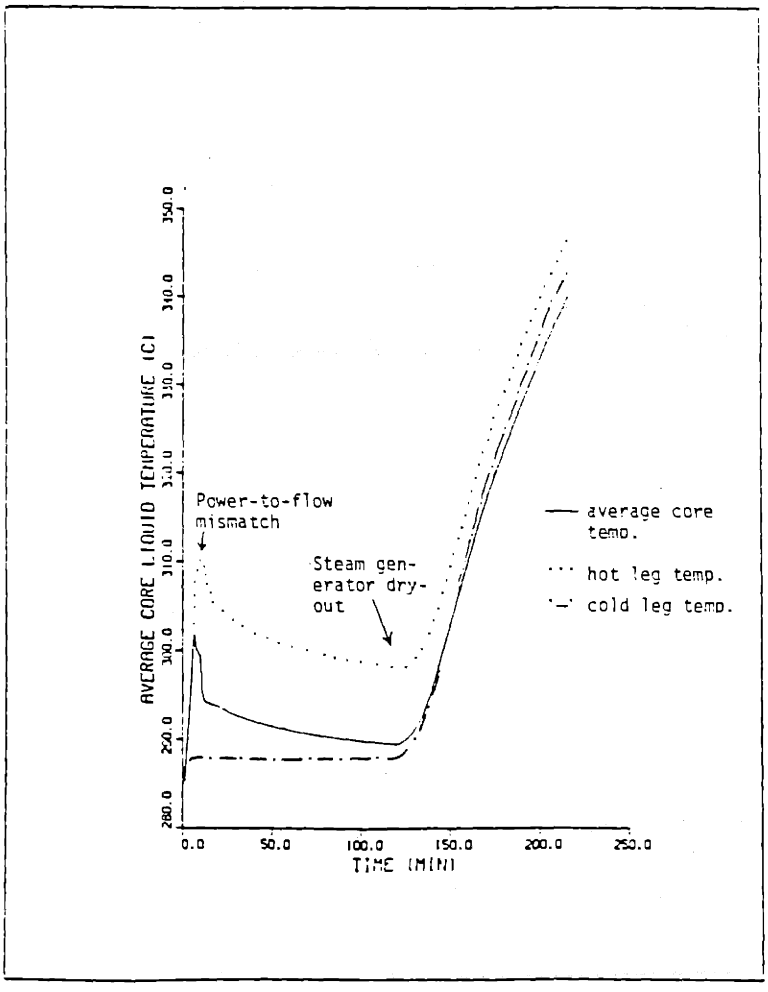

Figure 3-14 After steam generator dryout, the primary temperature increases until saturation at 219 min.

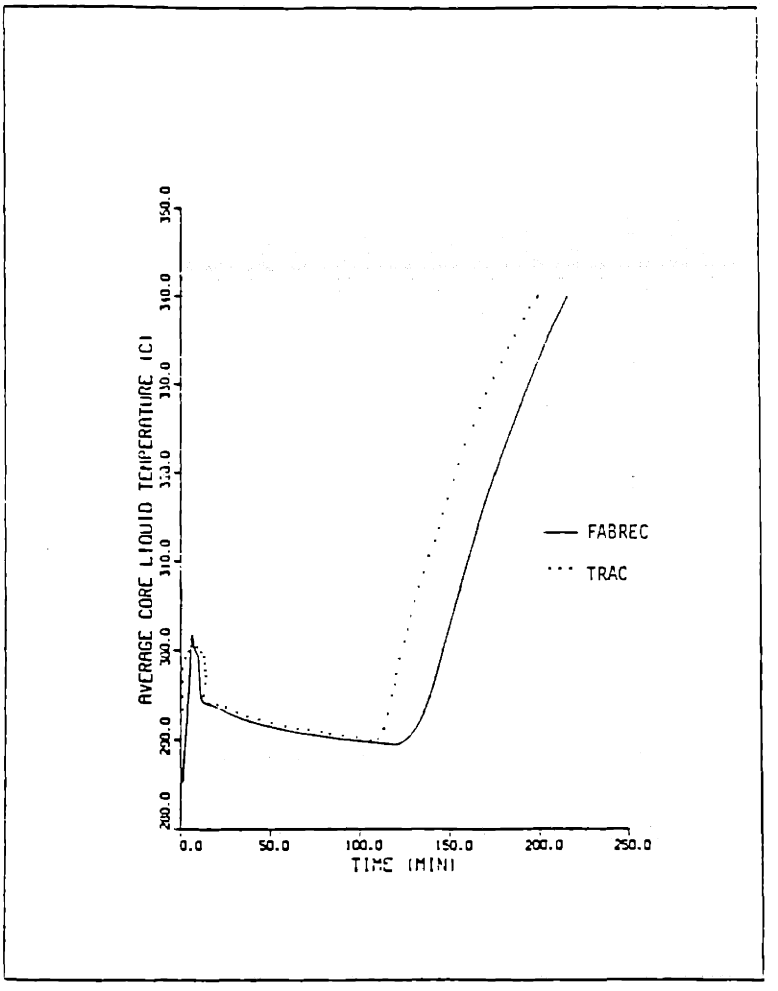

Figure 3-15 Comparison of the liquid temperature in the core predicted by TRAC and FABREC.

Table 3.1 Event Sequence for Loss-of-Feedwater Transient with no ECC Injection

Time (s)	Time (min)	Event
0.0		Loss-of-offsite power, reactor coolant pump trip, main feedwater pump trip, scram signal generated.
0.6		Reactor Scram.
	75	Degraded primary to secondary heat transfer.
	93	PORV setpoint pressure (16.1 MPa) reached.
	100	Solid pressurizer.
	114	Primary begins to void.
	119	SRV setpoint pressure (17.13 MPa) reached.
	128	End of calculation, core empty.

Table 3.2 Event Sequence for Loss-of-Feedwater with ECC Feed and Bleed Manually Initiated at 10 Minutes

Time (s)	Time (min)	Event
0.0		Loss-of-offsite power, reactor coolant pump trip, main feedwater pump trip, scram signal generated.
0.6		Reactor Scram.
	10	ECC injection manually initiated.
	18	PORV setpoint pressure reached (16.1 MPa).
	25	Solid pressurizer.
	145	Steam generator dryout.
	219	End of calculation, upper saturated, decay power at a level that is removable by ECC flow.

Section 4

FEED AND BLEED ANALYZED UNDER UNCERTAINTY

4.1 Introduction and Selection of Response Variable

The modeling and analyses presented in the previous sections indicate that it is possible to cool the core with the feed and bleed procedure described, provided that the input and modeling exactly describe the physical processes of the procedure. This section discusses how uncertainties in the input parameters affect the confidence we associate with our answer.

The first problem we have is to choose the variable, sometimes called the "response", that determines whether the feed and bleed procedure is successful. From a simple steady-state analysis, mass and energy balances show that at the PORV setpoint pressure, ECC flow is inadequate to prevent the primary water from voiding. The Case 2 analysis of the previous section shows that once the water saturates in the primary, more energy was removed by the ECC flow than was added by the decay heat, and thus the core was cooled. On the basis of these facts, the response variable chosen to judge whether or not feed and bleed is successful is the net core heating at the time of primary saturation, $\dot{Q}_{net}$, which is defined as

$$\dot{Q}_{net} = \dot{Q}_d - \dot{m}_{il}(h_g - h_{i\ell}). \qquad (4.1\text{-}1)$$

The first term on the right is the decay power at the time of primary saturation, and the second term represents the energy removed from the vessel by the ECC flow once the upper plenum has saturated. If $\dot{Q}_{net}$ is greater than zero, the feed and bleed procedure is not adequately cooling the core, and inversely, if $\dot{Q}_{net}$ is less than or equal to zero, the feed and bleed procedure is successful. A qualitative graphical representation of $\dot{Q}_{net}$ is shown in Figure 4-1.

4.2 Propagation of Uncertainties

The response variable, $\dot{Q}_{net}$, can be represented by a multivariate function,

$$\dot{Q}_{net} = S(x_1, x_2, \ldots, x_n) = S(\underline{X}). \qquad (4.2\text{-}1)$$

If the elements of input vector $\underline{X}$ are not single valued variables, but instead are random variables, then the output variable $\dot{Q}_{net}$ is also a random variable. If S were a simple closed form function, the distribution of $\dot{Q}_{net}$ could be analytically determined if the distribution of the inputs were known. The function S is, however, generated by the thermal hydraulic code FABREC and thus no closed form representation of S is available. If the closed form expression is not simple enough for an analytical solution, the numerical technique of the Monte Carlo simulation can be used. In this method, a large number of trials are performed, each trial consisting of one set of x_j's. The x_j's for each trial are chosen by random sampling techniques, from the known probability distribution function (pdf) of each x_j.

Monte Carlo simulations are possible even if a closed form expression for the random function is not available. In the case of $\dot{Q}_{net}$, each trial would be one run of FABREC. Although FABREC is relatively inexpensive to run, when multiplied by the thousands of trials necessary to obtain an accurate distribution for the output, the cost becomes prohibitive. The need for a closed form analytical expression of $\dot{Q}_{net}$ therefore remains. Such an analytical representation of S can be generated by the "respone surface" technique.

4.3 Response Surface Methods

In general terms, a response surface may be generated whenever the functional relationship between the output variable and input parameters is only known through a deterministic code (such as FABREC). In order to reduce the cost of running expensive computer programs many times as would be done in a Monte Carlo simulation, probabilistic response surface techniques have been developed (Ref.21). The procedure is to first input selected combinations of input parameters into the deterministic code. These outputs generated are then used to generate a response surface, which is substituted for the code in the Monte Carlo simulation.

A second degree polynomial, as presented in Ref.21, is used to generate the response surface for $\dot{Q}_{net}$. The polynomial has the following form

$$S(\underline{X}) = A + \sum_{j=1}^{n} \left\{ [B_j + C_j(x_j - x_{jo}) + \sum_{k=j+1}^{n} D_{jk}(x_k - x_{ko})](x_j - x_{jo}) \right\} \quad (4.3\text{-}1)$$

If $\underline{X}$ has n elements, then the number of coefficients unknown is given by

$$m = 1+2n+[n(n-1)/2] \quad (4.3\text{-}2)$$

$$= \frac{n^2}{2} + \frac{3}{2} n+1 \quad ;$$

therefore, m computer runs would be necessary.

For each input parameter, three values must first be chosen. The three values must represent the range of the parameter of interest. Typically, x_{jo} is chosen as the mean, x_{j1} as the lower limit, and x_{j2} as the upper limit. The response surface output will exactly fit that of the deterministic code at these points, which are known as "knot points".

The coefficients to (4.3-1) are generated first by perturbing one input parameter at a time and then by perturbing two at a time. The base case is that of no perturbation, i.e., $\underline{X}=\underline{X}_o=(x_{10},x_{20},\ldots,x_{no})$. If

we let S_o be the base case, $S_{1(j)}$ be the ouput calculated by setting $x_j=x_{j1}$, $S_{2(j)}$ determined from $x_j=x_{j2}$, and $S_{11(j,k)}$ be the output of $x_j=x_{j1}$, $x_k=x_{k1}$, then the coefficients to (4.3-1) can be calculated from the following equations

$$A = S_o \ , \tag{4.3-3}$$

$$B_j = R_{j1}(x_{jo}-x_{j2})+R_{j2}(x_{jo}-x_{j1}) \ , \tag{4.3-4}$$

and

$$C_j = R_{j1}+R_{j2} \ , \tag{4.3-5}$$

where

$$R_{j1} = \frac{S_{2(j)}-S_o}{(x_{j1}-x_{jo})(x_{j1}-x_{j2})} \ , \tag{4.3-6}$$

$$R_{j2} = \frac{S_{2(j)}-S_o}{(x_{j2}-x_{jo})(x_{j2}-x_{j1})} \ , \tag{4.3-7}$$

and

$$D_{jk} = \frac{S_o+S_{11(j,k)}-S_{1(j)}-S_{1(k)}}{(x_{j1}-x_{jo})(x_{k1}-x_{ko})} \ . \tag{4.3-8}$$

The elements of $\underline{X}$ not explicitly given as arguments of $S(\underline{X})$ are set equal to their reference (x_{jo}) value.

4.4 Selection of Input Variables and Response Surface Generation

Theoretically, any input parameter about which there is any uncertainty should be included in our response surface. Realistically, the cost of generating the response surface is proportional to m, the number of undetermined coefficients in (4.3-1). From (4.3-2), we see that the number of computer runs necessary to correlate just 20 input variables (n=20) is 231. It is wise to only include those variables that both significantly affect the output variable, $\dot{Q}_{net}$, and have a significant associated uncertainty.

The initial reactor power level is a such variable since the decay power is directly proportional to this initial level. The higher the initial level, the higher $\dot{Q}_{net}$ will be.

Another less obvious, but important input variable is the PORV setpoint pressure. This variable is important because once the pressurizer goes solid, the setpoint determines the system pressure. This directly affects the flow capability of the ECC pumps. If the setpoint were to drift high, the ECC flow would be reduced, increasing $\dot{Q}_{net}$.

The time at which the operator begins the feed and bleed is also important. Basically, the longer the delay before initiation of the procedure, the faster the steam generator secondary water inventory will be depleted. After the steam generators dry out, the primary saturates. This means that early feed and bleed initiation results in a longer time until the primary begin to void. Because the decay power decreases with time, the longer it takes for the primary to saturate, the less the net core heating, $\dot{Q}_{net}$, will be.

After the initial loss-of-offsite power, there is a time delay before the reactor is scrammed. The delay is the finite amount of time it takes to detect the event and generate a scram signal. This quantity is important because before the reactor is scrammed, its full-power level is boiling off the water inventory in the steam generator secondaries.

It was already determined that the PORV setpoint pressure is important because it determines where along the head-flow curve the ECC pumps will operate. Another important input parameter might reflect uncertainty in the actual head-flow curve. This would also affect the ECC flow into the primary system and thus the feed and bleed cooling capability.

Thus, we now have five important input parameters about which there is uncertainty. Using (4.3-2), we see that the number of computer runs necessary to generate the coefficients for our response surface is 21. The mean and limits of the variables are listed in Table 4.1. Using these inputs, FABREC generated the outputs listed in Table 4.2. Table 4.3 shows the coefficients to (4.3-1) calculated for these outputs.

4.5 Input Distributions and Monte Carlo Simulation

The uncertainties in the input variables are quantified by considering the latter as random variables with associated probability distributions. Table 4.4 lists the distribution chosen for each input and the parameters necessary to describe the distribution. For example, the initial power level is assumed to be normally distributed with a mean and standard deviation equal to that listed in the table. The scram delay was assumed to be log-normally distributed since this distribution is skewed to the left, and it has a finite lower limit. The time to initiate the ECC flow was assumed to be exponentially distributed with a time constant equal to the mean value of 10 min. The remaining variables are assumed to be normally distributed. The distribution parameters (with the exception of the exponential distribution) were chosen such that the lower and upper limits listed in Table 4.1, which were obtained from engineering judgement, represent the 1st and 99th percentiles of the pdf, i.e.,

$$\int_{-\infty}^{x_{j1}} f(x)dx = .01 \qquad (4.5\text{-}1)$$

and

$$\int_{-\infty}^{x_{j2}} f(x)dx = .99 \quad . \qquad (4.5\text{-}2)$$

Suppose we have a density distribution, f(x). What we need to do is find a procedure to generate x's such that they are distributed according to f(x). We do this by a one-variable transformation of a different density distribution, h(u).

Suppose h(u) is a uniform distribution that extends from 0 to 1. For $0<u<1$, h is independent of u (constant). The inverse function, $h^{-1}(u)$, is thus a random number generator of range 0 to 1 since h(u)du is constant in that range.

If we wish to map the function h(u) onto f(x), we can use the relation

$$f(x)dx = h(u)du \ , \tag{4.5-1}$$

or rearranging,

$$f(x) = h(u) \frac{du}{dx} \ . \tag{4.5-2}$$

Integrating from the lower limit yields

$$\int_{x_\ell}^{x} f(x')dx' = \int_{o}^{u} du' \ , \tag{4.5-3}$$

where x_ℓ is the lower limit of the f(x) distribution. Recognizing that the left-hand side of (4.5-3) is simply the cumulative distribution function, we can write

$$F(x) = u \ . \tag{4.5-4}$$

Solving for x yields

$$x = F^{-1}(u) \ . \tag{4.5-5}$$

Thus, to generate a sample of x's that are distributed according to F(x), one first generates the random number u and inputs this into the inverse cumulative function, F^{-1}.

Figure 4-2 is a histogram of a 10,000 trial Monte Carlo simulation of $\dot{Q}_{net}$. Since the success criterion is a non-positive $\dot{Q}_{net}$, the probability for success is represented by the area to the left of $\dot{Q}_{net}=0$, and similarly, the failure probability the area to the right of $\dot{Q}_{net}=0$. For the feed and bleed scenario studied, the success probability is .6373 and the failure probability is .3627.

4.6 Moment Matching $\dot{Q}_{net}$

Now that we have the histogram for $\dot{Q}_{net}$, we may wish to approximate it with a probability density function for which we have an analytical expression. The procedure that was used is called the "moment-matching method", and is described by Papazoglou and Gyftopoulos (Ref.10).

One way to describe our histogram is through its moments. For a discrete random variable, its r^{th} moment is defined as

$$M_r = \sum_{i=1}^{n} x_i{}^r f(x_i) \ . \tag{4.6-1}$$

For a continuous random variable,

$$M_r = \int_{-\infty}^{+\infty} x^r f(x)dx \ . \tag{4.6-2}$$

The first moment is the expected value, sometimes called the mean, and given the symbol μ.

$$M_1 = E(x) = \mu \tag{4.6-3}$$

We can also compute moments about the mean, sometimes called "central moments". They are defined as

$$M_r' = \Sigma(x_i-\mu)^r f(x_i) \tag{4.6-4}$$

for a discrete random variable, and

$$M_r' = \int_{-\infty}^{\infty} (x-\mu)^r f(x)dx \tag{4.6-5}$$

for a continuous random variable. The second central moment is called the variance of x. The square root of the variance is called the standard deviation of x, σ. Thus, we can write

$$M_2' = \text{var } x = \sigma^2 \ . \qquad (4.6\text{-}6)$$

The procedure for approximating the distribution of $\dot{Q}_{net}$ will be to first calculate its mean and second through fourth central moments. The third and fourth moments will be used to determine the type of distribution. The mean and variance will then determine the parameters for the distribution chosen.

The third central moment is called the "skewness", and is a measure of the asymmetry of the distribution. The fourth central moment is called the "kurtosis", and is a measure of its peakedness. These moments are used to define the following coefficients.

$$\text{coefficent of skewness: } \beta_1 = \frac{(M_3')^2}{(M_2')^3} \qquad (4.6\text{-}7)$$

$$\text{coefficient of kurtosis: } \beta_2 = \frac{M_4'}{(M_2')^2} \qquad (4.6\text{-}8)$$

Once β_1 and β_2 are calculated, one looks at Figure 4-3 to determine the appropriate distribution with which to fit the Monte Carlo simulation. Table 4.6 compares the cumulative probabilities for the exact and fitted results.

Based on these results, it is concluded that for the input parameter distributions chosen, $\dot{Q}_{net}$, representing the net core heating of the time the primary system water saturates, can be approximated by a normal distribution with a mean of -.573 MW, and a standard deviation of 1.58 MW. The probability of success (the probability that $\dot{Q}_{net} \leq 0$) is 64% for this distribution.

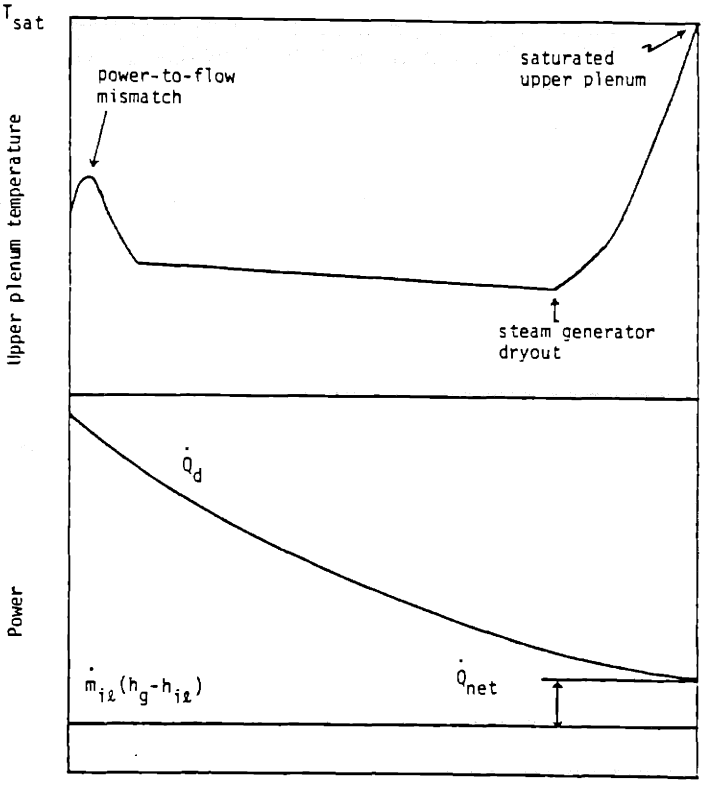

Figure 4-1 Qualitative graphical representation of $\dot{Q}_{net}$. As shown, Q_{net} represents the difference between the decay power and the power removed by the ECC flow at the time that the upper plenum saturates.

Figure 4-2 Histogram of $\dot{Q}_{net}$ generated by 10,000 trial Monte Carlo simulation.

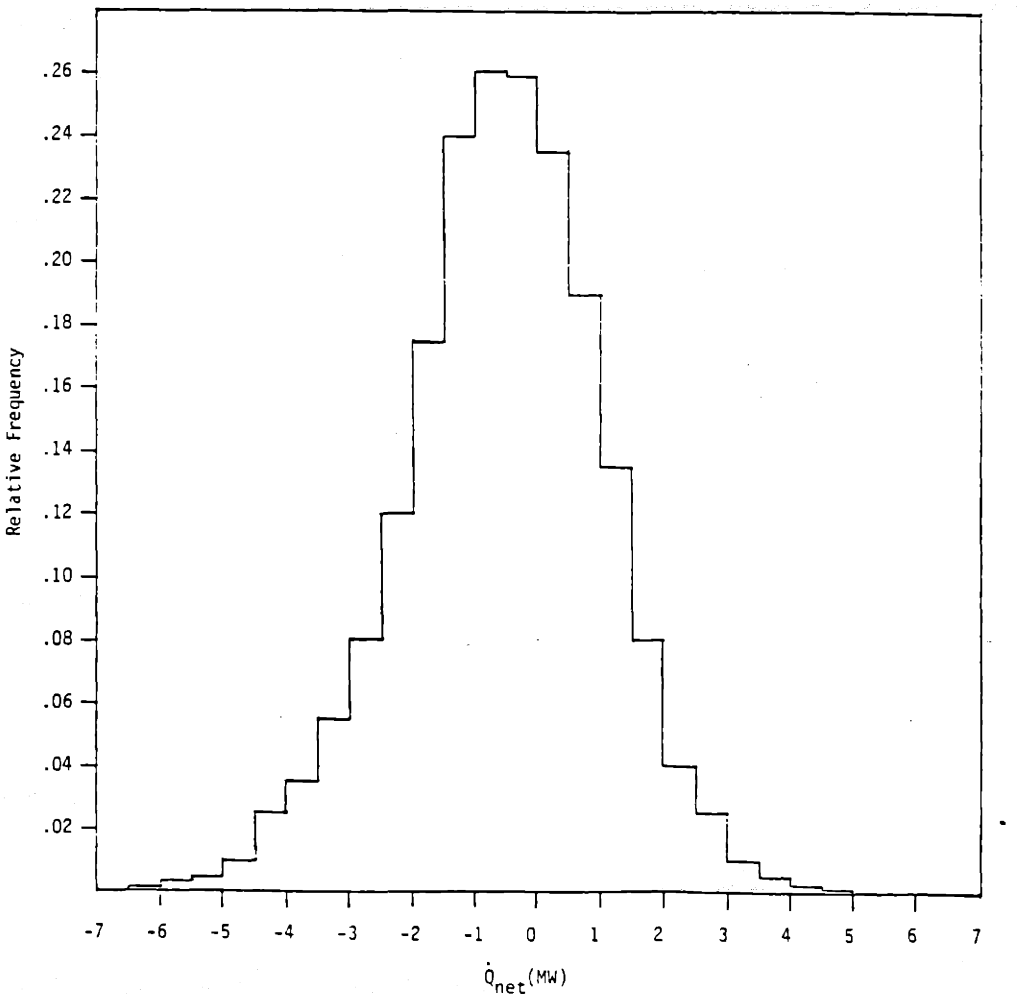

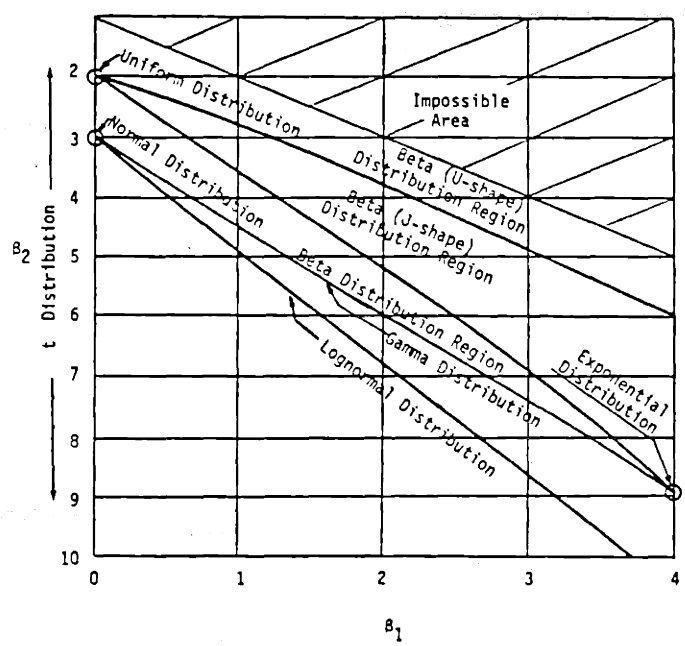

Figure 4-3 Region in (β_1,β_2) plane for various distributions.

Figure 4-4 Comparison of 10,000 trial Monte Carlo histogram with normal distribution approximation.

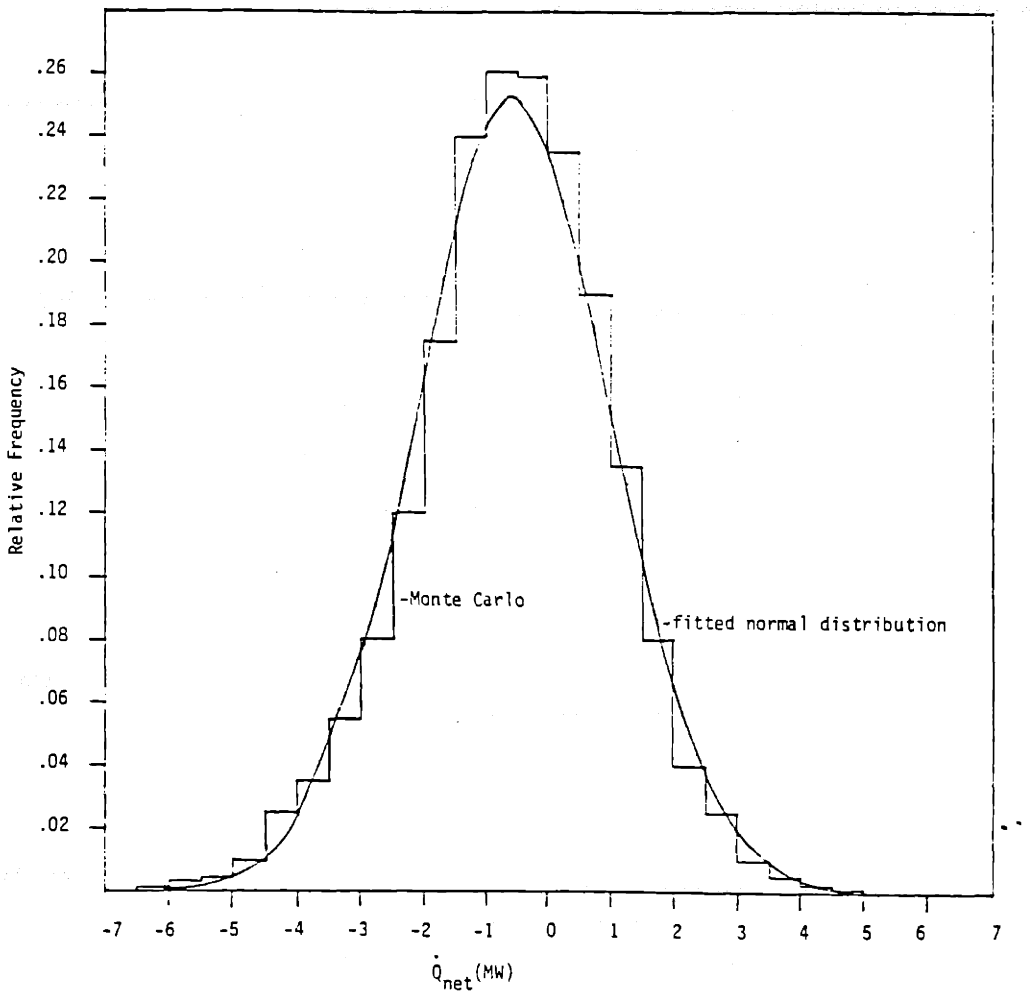

Table 4.1 Coordinates of Knot Points for Response Surface of $\dot{Q}_{net}$

Input Parmeter	Mean	Lower Limit	Upper Limit
Initial power (% of nominal)	100	95	105
PORV setpoint (MPa)	16.1	16.0	16.2
ECC initiation time (min)	10	5	60
Scram delay (s)	.6	.5	2
ECC flow curve (% of nominal)	100	95	105

Table 4.2 FABREC Outputs for Knot Point Coordinates

$\dot{Q}_{net}$(kW)

S_o = -436.94

$S_1(1)$	-4373.31	$S_2(1)$	1561.6
$S_1(2)$	-1412.6	$S_2(2)$	308.88
$S_1(3)$	-671.6	$S_2(3)$	2107.63
$S_1(4)$	-449.94	$S_2(4)$	-280.40
$S_1(5)$	1520.97	$S_2(5)$	-2443.14

$S_{11(j,k)}$

	(2)	(3)	(4)	(5)
(1)	-5143.6	-4598.4	-4390.9	-2254.8
(2)		-1420.79	5737.21	3984.0
(3)			-684.51	1555.65
(4)				1508.33

Table 4.3 Coefficients for Response Surface of $\dot{Q}_{net}$(kW)

A = -436.94

	$B_{(j)}$	$C_{(j)}$
(1)	5.935E4	-3.875E5
(2)	8.604E3	-1.146E-4
(3)	4.723E1	7.199E-2
(4)	1.288E2	-1.213E1
(5)	-3.964E4	-9.630E3

$D_{(j,k)}$

	(2)	(3)	(4)	(5)
(1)	4.10E4	3.828E1	-9.18E2	6.424E4
(2)		4.529E2	4.90E2	1.083E-5
(3)			1.8E-1	-3.912E2
(4)				7.2E1

Table 4.4 Distribution of Input Variables

Parameter	Distribution Type	Distribution Parameters
Initial power (% of nominal)	Normal	μ=100, σ=2
PORV setpoint (MPa)	Normal	μ=16.1, σ=.04
ECC initiation time (min)	Exponential	λ=1/ =.1
Scram delay (s)	Log normal	μ=-2.303, σ=1
ECC flow curve (% of nominal)	Normal	μ=100, σ=2

Table 4.5 Calculated Moments Monte Carlo Simulation of $\dot{Q}_{net}$ with 10,000 Trials

Mean	-.573
Variance	2.498
Third central moment	-.738
Fourth central moment	21.805

$$\beta_1 = .0350$$

$$\beta_2 = 3.4938$$

Table 4.6 Comparison of Cumulative Probabilities for Monte Carlo (10,000 trials) and Fitted Normal Distribution

$$F(x) = \int_{-\infty}^{x} f(x')dx'$$

$x=\dot{Q}_{net}$(MW)	F(x)	
	Monte Carlo	Fitted Normal
-4	.0220	.01508
-3	.0672	.06234
-2	.1690	.1833
-1	.3769	.3936
0	.6374	.6414
1	.8506	.8401
2	.9576	.9481
3	.9897	.9880
4	.9973	.9981
5	.9992	.9998

Section 5

CONCLUSIONS

The purpose of this study was to examine the feed and bleed process in a PWR in a probabilistic manner. Although best-estimate calculations performed in this study and elsewhere indicate that feed and bleed can successfully cool the core, this study explores how this answer may change when the input parameters vary from the values chosen in the best-estimate predictions. The input parameters were considered to be random variables with associated probability density functions. These uncertainties associated with these input parameters were then propagated to determine the uncertainty in the success of the feed and bleed process.

The first part of this study developed the modeling used in a best-estimate transient analysis code called FABREC. The code is fast running and can predict phenomena such as steam generator dryout times, natural circulation flow rates, and decay power levels. Because it is fast running, it is ideal for sensitivity studies.

The Zion-1 PWR was chosen as the plant to analyze. This is a four-loop Westinghouse reactor owned and operated by Commonwealth Edison. Because it has safety-grade charging as part of its ECCS, the feed and bleed scenario examined did not include latching open the PORVs to depressurize, or otherwise altering the PORV setpoint pressure from its normal value of 16.1 MPa. FABREC predicted that if the feed and bleed was initiated at 10 min, the primary would saturate at 219 min, at which time the ECC flow would remove energy at a rate of 29.0 MW. Since the core power at this time would be 28.6 MW, the core would be successfully cooled.

Uncertainties in five input parameters were considered to significantly affect the output variable, which was chosen to be the difference between the power added by the decay heat and the power removed by the ECC flow at the time of saturation of the primary fluid ($\dot{Q}_{net}$). The parameters varied were the initial power level, the PORV setpoint

pressure, the ECC initiation time, the scram delay time, and the ECC flow rate. Distributions were then chosen for these parameters such that the 1st and 99th percentile of the distribution represented the upper and lower limits of the input parameter, except for the parameter describing the ECC initiation time. For this parameter, the pdf was the exponential distribution with a time constant equal to the mean ECC initiation time.

A Monte Carlo simulation was performed to find the distribution of the output variable, Q_{net}, based on the input parameter distribution chosen. Although FABREC is fast running, it would still be cost prohibitive to use it directly in a Monte Carlo simulation. Instead a response surface was generated and that was used for the simulation.

After the distribution of $\dot{Q}_{net}$ was obtained from the Monte Carlo simulation, it was approximated by a pdf by matching its first four moments. Based on this moment matching technique, the distribution for $\dot{Q}_{net}$ was approximated by a normal distribution of mean equal to -.573 MW with a standard deviation of 1.58 MW.

For successful cooling of the core using feed and bleed, the requirement that the energy rate removed by the ECC flow exceed that of the core decay power implies that $\dot{Q}_{net}$ be less than zero. For the distribution generated, the probability of adequately cooling the core using the feed and bleed procedure is 64%.

Section 6

REFERENCES

1. Abdollahian, P., et al., "Prediction of critical flow rates through power-operated valves," presented at the 2nd International Topical Meeting on Nuclear Reactor Thermal Hydraulics, Santa Barbara, California, January 1983.

2. Chu, T. L., Apostolakis, G. E., "Time Dependent Accident Sequence Analysis," UCLA-ENG-83-15, March 1983.

3. "Decay Heat Power in Light Water Reactors," ANSI/ANS-5.1-1979.

4. DeMuth, N. S., et al, "Loss of Feedwater Transients for the Zion-1 Pressurized Water Reactor," Los Alamos National Laboratory, NUREG/CR-2656, May 1982.

5. Goldstein, R., et al., "Development of Reload Safety Analysis Methodology and Code Package Uncertainty Analysis: Amplification of Statistical Bases," Combustion Engineering, NP-2657, Dec. 1982.

6. Iannello, V., Todreas, N. E., "Steady-State Analysis of Feed and Bleed in PWR Systems," Special Problem in Nuclear Engineering, MIT, August 1983.

7. Keenan, J. H., Keyes, F. G., et al., Steam Tables, John Wiley and Sons, 1978.

8. Liles, D. R., et al., "TRAC-PD2, An Advanced Best-Estimate Computer Program for Pressurized Water Reactor Loss-of-Coolant Accident Analysis," Los Alamos Scientific Laboratory.

9. Martz, H. F., et al., "A Comparison of Methods for Uncertainty Analysis of Nuclear Power Plant Safety System Fault Tree Models," Los Alamos National Laboratory, NUREG/CR-3263, LA-9729-MS, April 1983.

10. Papazoglou, I. A., Gyftopoulos, E. P., "Markovian Reliability Analysis Under Uncertainty with an Application on the Shutdown System of the Clinch River Breeder Reactor," Brookhaven National Laboratory, NUREG/CR-0405, BNL-NUREG-50864, Sept. 1978.

11. Sanchez-Pope, A. E., "Quick-Look Report on OECD LOFT Nuclear Experiment LP-FW-1 (Loss of Feedwater)," Idaho National Engineering Laboratory, OECD LOFT-T-3104, March 1983.

12. Sheron, B. W., "Bases and Criteria for the Selection of Response Surface Parameters for the Statistical Assessment of a LOCA," ANS-ENS Topical Meeting on Probabilistic Analysis of Nuclear Reactor Safety, Los Angeles, 1978.

13. Shimeck, D. J., et al., "Analysis of Primary Feed and Bleed in PWR Systems," Idaho National Engineering Laboratory, EGG-SEMI-6022, September 1982.

14. Shooman, M. L., Probabilistic Reliability: An Engineering Approach, McGraw-Hill, 1968.

15. "System Response to Total Loss of Steam Generator Heat Sink," Babcock and Wilcox Document 86-1103585-00, August 1979.

16. Smith, L. P., et al., "Modular Modeling System (MMS): A Code for the Dynamic Simulation of Fossil and Nuclear Power Plants," Electric Power Research Institute, CS/NP-2989, March 1983.

17. Tauche, W., "Loss of Feedwater Induces Loss of Coolant Accident Analysis Report," Westinghouse Nuclear Energy System, WCAP-9744, May 1980.

18. Todreas, N. E., Kazimi, M. S., "Nuclear Analysis Class Notes-Chapter 16," to be published.

19. Uppuluri, V. R. R., Kuo, W., "Survey of Error Propagation in Systems," Oak Ridge National Laboratory, NUREG/CR-2839, ORNL/CSD/TM-190.

20. VanTuyle, G. J., et al., "MINET-Transient Analysis of Fluid Flow and Heat Transfer Networks," BNL-NUREG-32858, Computers in Engineering Proceedings, Vol.1, p.289, August 1983.

21. Vaurio, J. K., "Response Surface Techniques Developed for Probabilistic Analysis of Accident Consequences," ANS-ENS Topical Meeting on Probabilistic Analysis of Nuclear Reactor Safety, Los Angeles, 1978.

22. Wooton, R. O., Arci, H. I., "MARCH (Meltdown Accident Response Characteristics) User's Manual," NUREG/CR-1711, October 1980.

23. "Zion Station Final Safety Analysis Report," Commonwealth Edison, 1973.

24. Zvirin, Y., "A Review of Natural Circulation Loops in Pressurized Water Reactors and Other Systems," Nuclear Engineering Design, 67, pp.203-225, 1981.

APPENDIX: Derivation of Pressurizer Equations

In this derivation, the pressurizer is assumed to be in thermal equilibrium and thus the pressure determines the thermodynamic state of both the saturated vapor and saturated liquid phases. The derivationis based on the mass, energy, and volume equations for the combined vapor and liquid, which are

$$\dot{m}_f+\dot{m}_g = \dot{m}_{up}-\dot{m}_{porv}-\dot{m}_{srv} \quad , \tag{1}$$

$$\dot{m}_f u_f+m_f\dot{u}_f+\dot{m}_g u_g+m_g\dot{u}_g = \dot{m}_{up}h_{up}-\dot{m}_{porv}-h_{porv}-\dot{m}_{srv}h_{srv} \quad , \tag{2}$$

$$\dot{m}_f v_f+m_f\dot{v}_f+\dot{m}_g v_g+m_g\dot{v}_g = 0 \quad . \tag{3}$$

Solving (1) for $\dot{m}_f$ and substituting into (3) yields

$$\dot{m}_f = \dot{m}_{surge}-\dot{m}_{porv}-\dot{m}_{srv}-\dot{m}_g \quad , \tag{4}$$

$$m_f\dot{v}_f+\dot{m}_{up}v_f-\dot{m}_{porv}v_f-\dot{m}_{srv}v_f-\dot{m}_g v_f+\dot{m}_g v_g+m_g\dot{v}_g = 0. \tag{5}$$

We can solve (5) for $\dot{m}_g$ to obtain

$$\dot{m}_g = \frac{(\dot{m}_{porv}+\dot{m}_{srv})v_f-m_f\dot{v}_f-\dot{m}_{up}v_f-m_g\dot{v}_g}{v_g-v_f} \tag{6}$$

For a saturated liquid or vapor,

$$\frac{d\Delta}{dt} = \left(\frac{d\Delta}{dp}\right)\frac{dp}{dt} \quad , \tag{7}$$

where Δ is an intensive thermodynamic property. Making use of (7) and (2) produces

$$\dot{m}_f u_f + m_f \left(\frac{du_f}{dp}\right)\dot{p} + \dot{m}_g u_g + m_g \left(\frac{du_g}{dp}\right)\dot{p} = \dot{m}_{up} h_{up} - \dot{m}_{porv} h_{porv} - \dot{m}_{srv} h_{srv} \quad (8)$$

We can solve (8) for $\dot{p}$,

$$\dot{p} = \frac{\dot{m}_{up} h_{up} - \dot{m}_{porv} h_{porv} - \dot{m}_{srv} h_{srv} - \dot{m}_f u_f - \dot{m}_g u_g}{m_f \left(\frac{du_f}{dp}\right) + m_g \left(\frac{du_g}{dp}\right)} \quad (9)$$

Substituting (4) and (6) into (9) results in

$$\dot{p} = \frac{\dot{m}_{up} h_{up} - \dot{m}_{porv} h_{porv} - \dot{m}_{srv} h_{srv} - \dot{m}_{up} u_f + \dot{m}_{porv} u_f + \dot{m}_{srv} u_f + \left(\frac{\dot{m}_{porv} v_f + \dot{m}_{srv} v_f - m_f \dot{v}_f - m_g \dot{v}_f - \dot{m}_{up} v_f}{v_g - v_f}\right)(u_f - u_g)}{m_f \frac{du_f}{dp} + m_g \frac{du_g}{dp}} \quad (10)$$

The final result is produced by using (7) to substitute for the rate of change of the specific volumes and then solving for p. The equation for p is

$$\dot{p} = \frac{\dot{m}_{up} h_{up} - \dot{m}_{porv} h_{porv} - \dot{m}_{srv} h_{srv} + u_f (\dot{m}_{porv} + \dot{m}_{srv} - \dot{m}_{up}) + (\dot{m}_{up} - \dot{m}_{porv} - \dot{m}_{srv})\left(\frac{v_f}{v_g - v_f}\right)(u_g - u_f)}{m_f \left(\frac{du_f}{dp}\right) + m_g \left(\frac{du_g}{dp}\right) - \left(\frac{dv_f}{dp}\right)\left(\frac{m_f u_g - m_f u_f}{v_g - v_f}\right) - \left(\frac{dv_g}{dp}\right)\left(\frac{m_g u_g - u_f}{v_g - v_f}\right)} \quad (11)$$

If we make the same substitution into (6), we obtain

$$\dot{m}_g = \frac{(\dot{m}_{porv}+\dot{m}_{srv})v_f - m_f(\frac{dv_f}{dp})\dot{p} - \dot{m}_{up}v_f - m_g(\frac{dv_g}{dp})\dot{p}}{v_g - v_f} \qquad (12)$$

Equations (11) and (12), together with (4), are the desired pressurizer equations.